Biochemical Journal (2020) **477** 407–429
https://doi.org/10.1042/BCJ20190706

PORTLAND PRESS

Research Article

A distinct concerted mechanism of structural dynamism defines activity of human serine protease HtrA3

Saujanya Acharya[1,2], Shubhankar Dutta[1] and Kakoli Bose[1,2]

[1]Advanced Centre for Treatment, Research and Education in Cancer (ACTREC), Tata Memorial Centre, Kharghar, Navi Mumbai 410210, India; [2]Homi Bhabha National Institute, Training School Complex, Anushaktinagar, Mumbai 400094, India

Correspondence: Kakoli Bose (kbose@actrec.gov.in)

Human HtrA3 (high-temperature requirement protease A3) is a trimeric multitasking pro-papoptotic serine protease associated with critical cellular functions and pathogenicity. Implicated in diseases including cancer and pre-eclampsia, its role as a tumor suppressor and potential therapeutic target cannot be ignored. Therefore, elucidating its mode of activation and regulatory switch becomes indispensable towards modulating its functions with desired effects for disease intervention. Using computational, biochemical and biophysical tools, we delineated the role of all domains, their combinations and the critical phenylalanine residues in regulating HtrA3 activity, oligomerization and specificity. Our findings underline the crucial roles of the N-terminus as well as the PDZ domain in oligomerization and formation of a catalytically competent enzyme, thus providing new insights into its structure–function coordination. Our study also reports an intricate ligand-induced allosteric switch, which redefines the existing hypothesis of HtrA3 activation besides opening up avenues for modulating protease activity favorably through suitable effector molecules.

Introduction

High-temperature requirement serine protease A3 (HtrA3), belongs to a family of unique homo-oligomeric and ATP-independent serine proteases that are known to perform a wide repertoire of biological functions such as mitochondrial homeostasis, unfolded protein response, cell growth and apoptosis [1]. While the prokaryotic HtrAs (e.g. DegP, DegQ and DegS) exhibit dual temperature-dependent chaperone–protease activity, their eukaryotic counterparts have evolved to undertake more intricate cellular functions [2]. Human HtrA proteins have been implicated in pathogenicity such as arthritis, cancer and neurodegenerative disorders [1]. These proteases are known for their structural complexity, which also results in their functional diversity. Their basic structure includes an N-terminal region, a serine protease domain (SPD) and one or more C-terminal post-synaptic density protein, Drosophila disc large tumor suppressor, zonula occludens-1 protein (PDZ) domain arranged in a pyramidal assembly ranging from trimers to large 24-mer oligomers [3–7]. The N-terminal region is variable among the family members and contains signaling as well as regulatory elements; the catalytic domain is represented by the chymotrypsin-like SPD while the PDZ is normally recruited for mediating protein–protein interactions [1]. The variations in the structural elements across the family, along with conformational dynamics and oligomeric assembly lead to subtle differences in their functionality, specificity and pathophysiology.

Among the four known human HtrA (HtrA1–4) proteases, HtrA-1, -3 and -4 share a common domain organization with a Kazal-like domain (KI) that acts as an inhibitor for serine protease activity, an insulin-like growth factor-binding protein domain (IGFBP) and a signal peptide at the N-terminus. HtrA2 (Omi) differs from the other members by the absence of the KI and IGFBP

Received: 22 September 2019
Revised: 20 December 2019
Accepted: 3 January 2020

Accepted Manuscript online: 3 January 2020
Version of Record published: 30 January 2020

Biochemical Journal (2020) 477 407–429
https://doi.org/10.1042/BCJ20190706

domains and is marked by the presence of an IAP (inhibitor of apoptosis) binding motif (IBM) and a transmembrane domain [8–10]. HtrA3 is synthesized as a 453 amino acid precursor protein, which consists of a signal peptide (1–17 residues), an IGFBP domain (21–77 residues), a KI (64–128 residues) domain, an SPD (175–340 residues) and one PDZ (359–444 residues) domain [1]. The active site residue Ser305 along with His191 and Asp227 form the catalytic triad. While HtrA1 and HtrA2 have been extensively characterized, HtrA3 and -4 are the relatively lesser studied members of this family. Briefly, literature available till date reports that the HtrA homologs assume a trimeric pyramidal architecture and exhibit similar mechanism of activation [11–17]. While HtrA-1, -2 and -4 have been reported to be allosterically activated [12,14,16], only one such study reports allostery in HtrA3 till date [18]. HtrA2, particularly, is allosterically regulated [12,14,16] through both the N- and C-terminal regions. The crystal structure of the substrate-unbound HtrA3 (3.27 Å) represents a trimeric pyramidal architecture with its orthosteric pocket buried 33 Å above the base of the pyramid [17]. This structural inaccessibility of the active site to the substrate or inhibitor molecules in the basal state hints towards the requirement of an allosteric mode of regulation for its activation. Moreover, the structure highlights three phenylalanine residues (F140, F142 and F255) from each monomeric chain that 'lock' together and might be crucial for stabilization of the trimer. However, the crystal structure does not satisfactorily define the important loops, especially the regulatory loop LA and the specificity/substrate binding loop L3 due to low electron density (high B factor). Therefore, despite providing an overview of HtrA3 spatial organization, this substrate-unbound structure fails to decipher the structural reorganizations and intrinsic conformational dynamics that lead to HtrA3 activation.

Human HtrAs are multitasking proteins, which are prominently involved in apoptosis and cell signaling [19–22]. HtrA1 and HtrA3 inhibit the TGF-β signaling pathway through a process dependent on their proteolytic activity [19,23]. Moreover, both these proteases have been reported to cleave several proteins *in vitro* such as decorin, biglycan, actin, β-tubulin, vimentin and TCP1α chaperonin, suggesting a role in the reorganization of extracellular environment [23,24]. In an apoptotic background, upon stress induction, a section of the N-terminal region of HtrA proteases harboring the mitochondrial localization signal gets cleaved leading to the formation of a 'mature' enzyme, which is subsequently translocated from the mitochondria to the cytoplasm to mediate apoptosis commonly through both caspase-dependent and independent mechanism [1,25–27]. HtrA2 and HtrA3 specifically bind and cleave XIAP (X-linked inhibitor of apoptosis) to trigger the caspase-mediated intrinsic pathway [22,28–32]. While HtrA2 binds XIAP via the tetrapeptide IBM (AVPS residues) that is exposed on maturation, no such sequence has been defined for HtrA3. Besides, their participation in non-classical cell death pathways has also been hypothesized [25,26,33].

HtrA3, first identified as a pregnancy-related serine protease (PRSP), plays an important role in regulating trophoblast invasion during placentation [10,34–37]. Research in the past few years has linked this protein to cancer development due to its involvement in apoptosis and cell signaling and it has recently emerged as a potential tumor suppressor [33]. Down-regulation of HtrA3 has been observed in several cancer cell lines and tumors such as ovarian, endometrial and lung cancers [38–40]. Furthermore, it has recently been shown that in lung cancer patients, HtrA3 suppresses tumor cell invasiveness through its proteolytic activity and sensitizes the cancer cells to death caused by chemotherapeutic drugs, such as cisplatin and etoposide [22,41]. Thus, its role as a potential therapeutic target cannot be repudiated. Therefore, its mode of activation and regulation needs to be elucidated in detail to be able to modulate its functions with desired effects for therapeutic benefit.

Here, we performed biochemical, biophysical, functional enzymolozy and *in silico* studies of 'mature' HtrA3, its different domains (individually and in various combinations) as well as its mutants to delineate the contribution of each structural component of the enzyme in defining oligomerization state, stability, substrate specificity and allosteric properties. Our findings highlight that activation of HtrA3 occurs through an intricate allosteric pathway. Contrary to previous reports [17], through in-depth enzymology and biophysical studies, we underscored the importance of the N-terminal, PDZ domain as well as the phenylalanine 'lock' residues in oligomerization and protease activity. Our *in silico* data clearly demonstrates that reorientations of the catalytic triad residues due to substrate binding culminate in a catalytically competent active site pocket. This process is impaired in its mutants and deletion variants, which has also been strengthened and validated by our *in vitro* studies. Therefore, these observations underline how the complex trimeric structure in concert with ligand-induced conformational dynamics and inter-domain coordination mediate HtrA3 function. In a nutshell, we provide a detailed understanding of the regulatory switch driving HtrA3 activation with the prospect of exploiting this information for devising therapeutic strategies against diseases it is associated with.

Biochemical Journal (2020) **477** 407–429
https://doi.org/10.1042/BCJ20190706

Experimental

Plasmid construction

HtrA3 cDNA comprising 1–453 amino acids (aa) in pDONR221vector was obtained from DNASU plasmid repository (The Biodesign Institute/Arizona State University). Different HtrA3 domains were subcloned between NdeI and BamHI restriction sites of bacterial expression vector pET-20b (New England Biolabs, Ipswich, U.S.A.) or pET-28a (New England Biolabs) or pMALc5E (New England Biolabs). While pET-20b has a C-terminal His_6-tag, pET-28a has both N and C-terminal His_6-tags, and pMALc5E provides an N-terminal maltose-binding protein (MBP) tag for easy purification of proteins through affinity chromatography.

Primers used for generating the different constructs have been listed in Table 1. Several other mutants of HtrA3 were generated using site-directed mutagenesis (Stratagene, Cedar Creek, TX, U.S.A.). The forward primers for the mutants HtrA3 S305A (active site mutant), HtrA3 F142D, HtrA3 F142A and HtrA3 F255D, respectively, are as follows:

5′-CAACTACGGGAACGCTGGGGGACCACTG-3′
5′-CGCTACAAGTTCAACGACATTGCTGACGTGGTG-3′
5′-CGCTACAAGTTCAACGCTATTGCTGACGTGGTG-3′
5′-GCGGCCTGGGGAGGACGTGGTGGCCATCG-3′

For all these mutants, the reverse primers are their complementary sequences. All HtrA3 variants were confirmed by DNA sequencing.

Protein expression and purification

Escherichia coli BL21 (DE3) (Novagen, Billerica, MA, U.S.A.) cells were transformed with expression plasmids and were grown at 37°C until OD_{600} of 0.6 was reached. Protein expression was then induced with 0.5 mM isopropyl-1-thio-D-galactopyranoside and cells were further cultured at 18°C for 20 h post induction. All His_6-tagged proteins were purified by affinity chromatography using Ni-IDA beads. Briefly, cells were lysed by sonication and the centrifuged supernatants containing the proteins with either C-terminal His_6-tags in pET-20b vector or C- and N-terminal His_6-tags in pET-28a vector were pre-equilibrated with nickel-IDA beads for 1 h at room temperature. The proteins of interest were then eluted using an Imidazole gradient. All purified proteins were >95% pure as estimated by SDS–PAGE. Eluted proteins were further purified using gel permeation chromatography.

Table 1 List of primers used for generating different HtrA3 domains and variants

Protein	Sequence (5′→3′)	Orientation
Mature HtrA3 (130–453)	CATATGCTCCACCAGCTGAGCAGCCCG	Forward
	GGATCCCATGACCACCTCAGGTGCGAG	Reverse
HtrA3 variant (135–453)	CATATG AGCCCGCGCTACAAGTTCAAC	Forward
	GGATCCCATGACCACCTCAGGTGCGATG	Reverse
HtrA3 variant (144–453)	CATATGGCTGACGTGGTGGAGAAGATC	Forward
	GGATCCCATGACCACCTCAGGTGCGATG	Reverse
HtrA3 N-SPD (130–340)	CATATGCTCCACCAGCTGAGCAGCCCG	Forward
	GGATCCGAACCGTGTGATGCGGTCTGAGGG	Reverse
HtrA3 SPD (175–340)	CATATGGGTTCTGGCTTCATCATGTCAG	Forward
	GGATCCGAACCGTGTGATGCGGTCTGAGGG	Reverse
HtrA3 SPD–PDZ (175–444)	CATATGGGTTCTGGCTTCATCATGTCAG	Forward
	GGATCCGAGGAGGTCGTCGTTCCCCCGC	Reverse
HtrA3 PDZ (359–444)	CATATGATACGGATGCGGACGATCACAC	Forward
	GGATCCGAGGAGGTCGTCGTTCCCCCGC	Reverse

Numbers indicate the start and end amino acid residues. The different domains include: Serine protease domain (SPD), N-terminus and SPD (N-SPD), SPD and PDZ domain (SPD–PDZ) and PDZ domain.

Biochemical Journal (2020) 477 407–429
https://doi.org/10.1042/BCJ20190706

The MBP-tagged domain (SPD) was purified using amylose resin (New England Biolabs) in the buffer: 20 mM Na_2HPO_4/NaH_2PO_4 (pH 8) containing 100 mM NaCl. The protein was eluted in 10 mM maltose and the MBP-tag was cleaved using TEV protease. This was further subjected to size exclusion chromatography. All of the fractions with >95% purity as estimated by SDS–PAGE were stored in aliquots at −80°C.

Size exclusion chromatography

Molecular mass and oligomeric property of HtrA3 variants were estimated by size exclusion chromatography. One milliliter of protein samples were run on Superdex 200 10/300 HR column and Superdex 200 10/300 GL column (GE Healthcare, Bjorkgatan, Uppsala, Sweden) pre-equilibrated with buffer comprising 20 mM Na_2HPO_4/NaH_2PO_4, 100 mM NaCl, pH 8.0 (buffer A) and eluted at a flow rate of 0.3 ml/min. The standards used for calibration were alcohol dehydrogenase (ADH), bovine serum albumin (BSA), lysozyme and MBP. All standards except for MBP which was laboratory purified, were purchased from Sigma Chemicals (St. Louis, MO, U.S.A.). Elution volume (V_e)/void volume (V_0) versus log of molecular mass of standards were plotted to generate the calibration curve from which molecular mass of HtrA3 variants were calculated.

Enzyme activity assays

The protease activity was determined using generic serine protease substrate β-casein (Sigma Chemicals). In one set of reactions, protease activity was analyzed over a range of substrate concentration. For each 30 μl reaction respective enzymes were incubated with 2–10 μg of β-casein in buffer A at 37°C for 2 h. In another set, protease activity was analyzed over a time range. Respective enzymes were incubated with 6 μg of β-casein in buffer A at 37°C for 0–2 h. The reactions were stopped with SDS–PAGE sample buffer and boiled for 5 min. The reaction products were analyzed by 10% or 12% SDS–PAGE followed by Coomassie Blue staining. Protease activity was also determined over a temperature range of 30–60°C for 2 h. For semi-quantitative analysis of protease activity, bands were quantified using Image J (1.47V, NIH, U.S.A.), and graphs were plotted using GraphPad Prism 6.

For all quantitative studies, FITC-labeled (fluorescein isothiocyanate) β-casein (Sigma Chemicals) was used and assays were performed as described subsequently. Fluorescent substrate cleavage was determined by incubating 2 μM of the enzyme with increasing concentration (0–10 μM) of FITC-β-casein at 37°C in cleavage buffer (buffer A). An increase in fluorescence was monitored in a multi-well plate reader (Berthold Technologies) using an excitation wavelength of 485 nm and emission at 545 nm.

Reaction rates V_0 (mM/min) were determined by linear regression analysis corresponding to the maximum reaction rates for individual assay condition. The steady-state kinetic parameters were obtained from the reaction rates by fitting data to modified Michaelis–Menten equation using nonlinear least-squares subroutine in KaleidaGraph program (Synergy software). V_{max} is the maximum velocity and $K_{0.5}$ is the substrate concentration at half-maximal velocity. All of the experiments were carried out independently in triplicates and the mean ± SEM values are reported in the results.

Fluorescence emission and far UV CD spectroscopy

Fluorescence emission was measured with protein solutions (2 μM) using Fluorolog-3 spectrofluorometer (HORIBA Scientific, Edison, NJ, U.S.A.) in buffer A with 295 nm excitation followed by emission between 310 and 400 nm. For Urea denaturation studies, 1 μM protein was denatured using 8 μM urea. Comparative emission scans of the denatured and refolded proteins were then recorded and the emission maxima were determined.

Far-UV CD scans were recorded between 260 and 190 nm with 10 or 20 μM protein solutions using a bandwidth of 1 nm and an integration time of 1 s in buffer A using Jasco J-815 spectropolarimeter (Jasco, Inc., Easton, MD, U.S.A.). Each spectrum was an average of five scans, with a scan rate of 20 nm/min. For thermal denaturation studies, Far UV CD experiments were performed between 20 and 100°C, where data were collected at 2°C intervals. Ellipticity corresponding to 222 or 208 nm at different temperatures was plotted against wavelength for calculation of melting temperature (T_m).

N-terminal sequencing

The substrate specificity of HtrA3 was determined by protein sequencing analysis using N-terminal Edman degradation. Generic serine protease substrate β-casein was used for this purpose. HtrA3 (4 μg) was incubated with β-casein (10 μg) in buffer A at 37°C for 1 h. The proteolytic products were analyzed on 12% Tris-tricine

gel and transferred onto PVDF membrane (Millipore Corporation, Billerica, MA, U.S.A.) using Bio-Rad wet transfer apparatus in 1X transfer buffer (25 mM Tris, 192 mM glycine, 20% (v/v) methanol, 0.025–0.1% SDS, pH 8.3) at a constant voltage of 20 V for 10 h. Transferred proteins (minimum amount ∼10–50 picomoles) were stained with 0.1% amido black, 25% isopropanol and 10% acetic acid solutions followed by destaining in 40% methanol and 10% acetic acid. The stained fragments were excised from the membrane and sent to protein sequencing facility for identification of five N-terminal amino acids by ABI 494 sequence pro^{TM} Protein sequencers (Tufts University Core Facility, Boston, MA, U.S.A.).

In silico preparation of models for mature HtrA3, HtrA3 N-SPD and its mutants

The structure of HtrA3 (PDB ID: **4RI0**) was retrieved from Protein Data Bank [17]. Since PDZ domain was missing from chains B and C of the trimeric HtrA3 structure, these were modeled with the help of Prime (Prime, Schrödinger, LLC, New York, NY, U.S.A., 2018) tool using the PDZ domain from chain A as a template [42]. In addition, few loop regions, such as^{130}LHQLS^{134} in chains A and C, as well as ^{163}HPLFGR^{168} and ^{277}AQREGRELGLRDS^{289} in all the chains were missing in the HtrA3 crystal structure. These missing regions were modeled and refined using loop filling and protein preparation programs in Prime (Prime, Schrödinger, LLC) [42,43]. Loop filling was done on the basis of permissive dihedral angle values for different residues, followed by repetitive rounds of sample loop clustering, optimizing the side-chain and energy minimization of the loops [42]. For the preparation of HtrA3 N-SPD monomer (130–340 aa), chain B from the modeled structure was used after removing the hinge region and the PDZ domain. The modeled structure was further subjected to two subsequent mutageneses in all the three chains using PyMOL (The PyMOL Molecular Graphics System, Version 2.0, Schrödinger, LLC), where F142 and F255 were mutated to aspartic acid to understand their importance in trimerization [44]. A305 amino acid residue in all these modeled proteins (phenylalanine mutants, HtrA3 N-SPD and mature HtrA3) was changed to serine to obtain the catalytically active form (S305 active site residue) prior to MD simulation analysis.

MD simulation analysis of mature HtrA3, its mutants, unbound HtrA3 N-SPD and peptide-bound HtrA3 N-SPD

Wild-type HtrA3 (mature), its mutants, unbound HtrA3 N-SPD and peptide-bound HtrA3 N-SPD were subjected to MD simulation using GROMACS 2018 where AMBER99sb-ILDNP force field was used to generate topology and parameter files [45,46]. Each protein was surrounded by a truncated octahedron box of TIP3P water molecules with the nearest distance from the protein to the box boundary being no more than 10 Å [47]. Since net charges for all the systems were less than zero, an adequate number of positive (Na^+) ions were added to each system for neutralization. Each system underwent one round of steepest-descent minimization and one round of conjugated gradient of 5000 steps [48]. Particle-mesh Ewald method (PME) was used for the calculation of electrostatic interactions and cut-off for Lennard–Jones interactions was set at 10 Å [49]. Throughout the simulation, to maintain constant temperature and pressure, V-rescale temperature coupling (a modified version of Berendsen thermostat) and Parrinello–Rahman pressure coupling were used [50,51]. For attaining favorable orientation of water molecules and Na^+ around the systems, they were subjected to equilibration, performed under NVT (N = number of particles, V = system's volume, T = absolute temperature) or isothermal-isochoric ensemble for 1 ns where the whole system was heated at 300 K [52]. This was followed by NPT (N = number of particles, P = system's pressure, T = absolute temperature) or isothermal-isobaric equilibration for 2 ns where pressure was kept constant at 1 atm with isothermal compressibility of solvent at 4.5×10^{-5} atm^{-1} and constant temperature of 300 K [52]. During equilibration, LINCS (LINear Constraint Solver) constraint algorithm was used to apply position restraining force on all the heavy atom bonds present in the system [53]. Finally, 100 ns MD simulation (production run) were conducted for HtrA3, its phenylalanine mutants, unbound HtrA3 N-SPD and bound HtrA3 N-SPD under NPT ensemble where co-ordinates were saved in every 1 ps of time interval. The resultant trajectories from the MD simulations were analyzed using energy, rms, rmsf, gyrate, sham, distance, bar and trjconv packages from GROMACS 2018 [45]. Clusters were generated at 100 ps intervals throughout the simulation, which gave a total of 5000 structures for HtrA3, its phenylalanine mutants, unbound HtrA3 N-SPD and bound HtrA3 N-SPD. Using the free energy landscape (FEL), the cluster representing the lowest energy conformers was extracted and analyzed on the basis of the cross-relation plot between RMSD (root mean squared deviation) and radius of gyration [54]. Comparisons among wild-type HtrA3 and its phenylalanine mutants were done based on their overall calculated RMSD,

Biochemical Journal (2020) **477** 407–429
https://doi.org/10.1042/BCJ20190706

residue-wise RMSF (root mean squared fluctuation) values, number of intramolecular hydrogen bonds and changes in the catalytic triad residues (H191, D227 and S305) distances [17]. For the comparison of peptide-bound and unbound HtrA3 N-SPD, overall RMSD, as well as domain-wise RMSD, were taken into consideration. All the graphs were plotted using XmGrace (ftp://plasma-gate.weizmann.ac.il/pub/grace/).

Results

Generation of different HtrA3 domains and variants

To understand the contribution of critical residues and domains in maintaining its overall structural integrity and functions, different mutants and variants of HtrA3 were generated (Figure 1A). Several literature reports highlight that the N-terminal region, as well as N-terminal aromatic residues, are crucial for maintaining the structure and regulating the enzymatic activity of HtrA family proteins [44]. It is also reported that the trimeric architecture of HtrA3 is stabilized through inter-molecular van der Waals interactions by three crucial aromatic

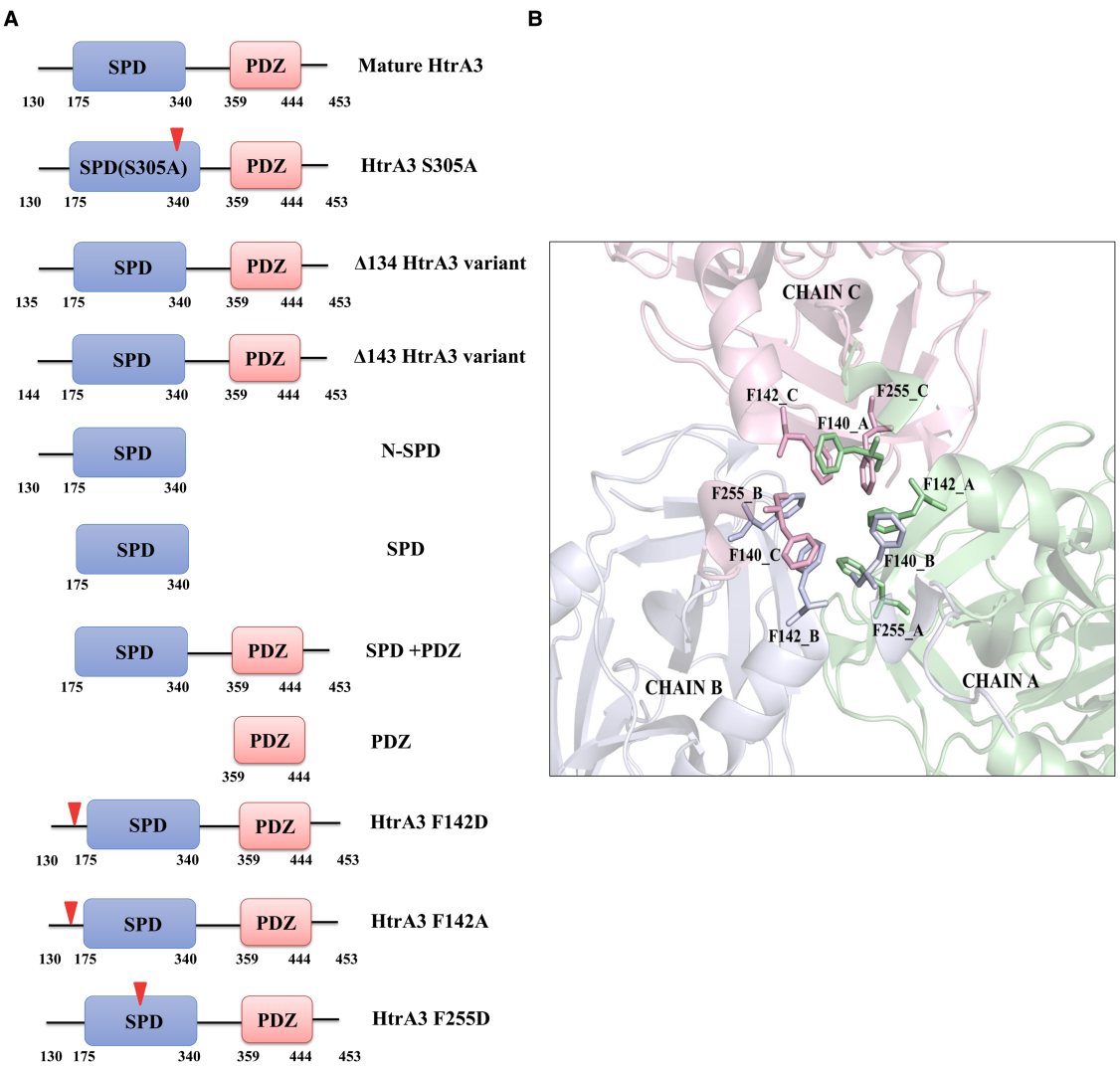

Figure 1. Schematic representation of different domains and mutants of HtrA3 generated for the present study.
(**A**) SPD indicates serine protease domain (175–340 residues); PDZ domain (359–444 residues); solid lines indicate N-terminal region (130–174 residues) and linker region (341–358 residues); triangles indicate positions of mutations on the respective domains or N-terminal region. (**B**) Ribbon diagram of the crystal structure of HtrA3 (PDB accession number 4RIO). Amino acid substitutions in HtrA3 protease are shown in stick models. Ribbon diagram was generated using PyMOL.

residues. The interaction of three phenylalanines from each monomer (F140, F142 and F255) forms a 'triple lock', which stabilizes the trimer similar to other proteins from HtrA family (Figure 1B).

These residues are also a part of the predicted homo-trimerization motifs based on sequence alignment with HtrA homologs [44]. One of these residues when mutated to aspartate (F142D) was found to disrupt these interactions and render the protein monomeric [32,44]. Therefore, to understand the importance of the 'phenylalanine-lock' residues as well as the role of N-terminal region in HtrA3 trimerization and activity, we made HtrA3 F142D, HtrA3 F142A and HtrA3 F255D single mutants, as well as a few N-terminal, deleted variants of the wild-type protein (Δ134 HtrA3 and Δ143 HtrA3) for our studies.

Along with these Phenylalanine single mutants, N-terminal deleted SPD–PDZ (HtrA3 SPD–PDZ) and PDZ (HtrA3 PDZ) variants were generated to understand the contribution of N-terminal region and SPD in structure, stability and protease activity. Similarly, an N-SPD (HtrA3 N-SPD, sans the PDZ domain) variant was also generated to investigate the role of PDZ in regulating oligomerization, protease activity and stability of HtrA3. This protein, on comparison with mature HtrA3, HtrA3 SPD–PDZ and the HtrA3 'lock' mutants, would highlight the importance of PDZ in HtrA3 structure, and regulation of its enzymatic activity. SPD (HtrA3 SPD) domain alone was purified separately to understand the roles of both N-terminal region and PDZ domain in proper active site formation, protein stability and hence maintaining the structural integrity of the protease. Active site mutant (HtrA3 S305A) alone was expressed and purified for various biophysical studies since the wild-type protein has a propensity to degrade as observed in other HtrAs. Moreover, it would also be required as a control in enzymatic studies.

Secondary and tertiary structural properties of HtrA3 mutants and domains

Mature HtrA3 and its variants were expressed and purified. Far UV CD studies were performed to determine their secondary structural properties. Mature HtrA3, Δ134 HtrA3 variant, active site mutant HtrA3 (S305A), monomeric mutant HtrA3 (F142D) as well as its domains SPD and PDZ, showed both α-helical and β-sheet characteristics as expected (Figure 2A,B). HtrA3 F142D, HtrA3 SPD and HtrA3 PDZ showed a decrease in α-helical and increase in β-sheet characteristics compared with the wild-type protein, which is suggestive of significant changes in their secondary structural properties that corroborate well with the available crystal structure.

Fluorescence emission studies between 310 and 400 nm were performed for mature HtrA3 and its active site mutant (S305A). Excitation of the single tryptophan residue (W352), which is situated at the hinge region between the SPD and PDZ in a fairly exposed environment, was done at 295 nm to characterize their overall tertiary structural properties. Mature HtrA3 (HtrA3 WT) showed almost no change in emission maxima (~342 nm) compared with its active site mutant (S305A) suggesting that the mutation did not perturb the structure of the protease (Figure 2C). Comparative emission scans of urea denatured HtrA3 S305A (emission maxima ~ 348 nm) and the native protein (emission maxima ~ 342 nm) showed a blue shift of the emission maxima by 6 nm for the native protein thereby demonstrating that the protein has a well-folded tertiary structure (Figure 2D).

The thermal stability of the variants was monitored using Far UV CD at a temperature range of 20–80°C. The ellipticity at 222 nm was used to plot the folded-fraction of the respective proteins as a function of temperature. Our results demonstrate that T_m (melting temperature) of HtrA3 S305A and HtrA3 PDZ are 63°C and 46°C, respectively (Figure 2E) suggesting that the removal of the N and SPD domains has a destabilizing effect on the protease. T_m for other variants such as N-SPD and Δ143 HtrA3 could not be calculated because these proteins either precipitated beyond 50°C or optimal concentration could not be achieved. This suggests all the domains including PDZ contribute to the protein stability in a co-ordinated manner.

Overall, these studies highlight that the purified HtrA3 variants were well folded as reflected in their secondary and tertiary structural characteristics. These studies also underscored the importance of N-terminal region, SPD and PDZ domains in maintaining protein stability.

PDZ domain is indispensable for optimal catalytic activation in HtrA3

It was previously determined that the activation of mature HtrA3 occurs allosterically [18]. To understand whether allosteric activation of HtrA3 requires any direct involvement of the C-terminal PDZ domain, we determined the enzymatic parameters for the PDZ-lacking variant (HtrA3 N-SPD) (Table 2). The plot of the reaction velocity against the corresponding substrate concentration was fitted with modified Michaelis–Menten equation that accommodates Hill's cooperativity parameters (Figure 3A). HtrA3 N-SPD cleaved β-casein with

Biochemical Journal (2020) **477** 407–429
https://doi.org/10.1042/BCJ20190706

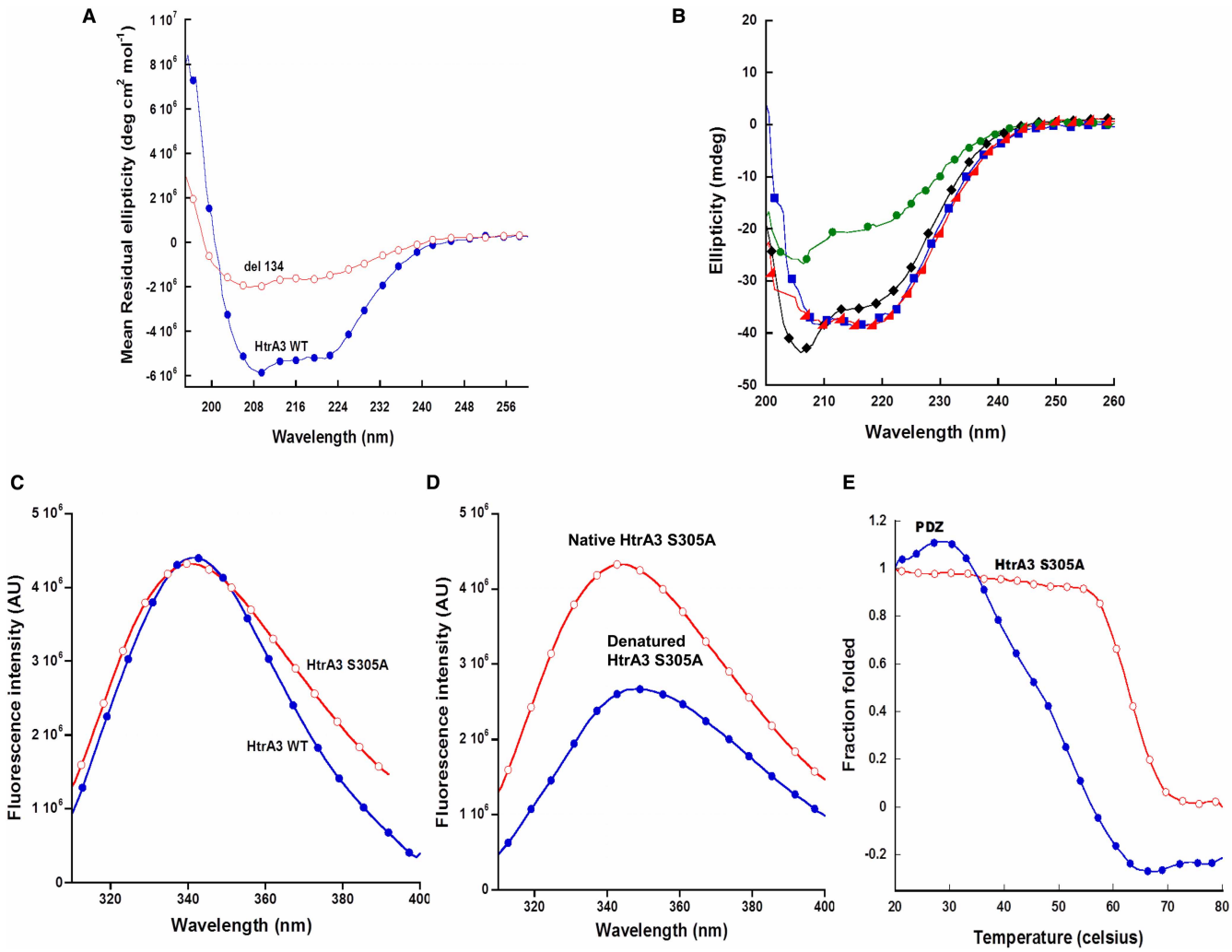

Figure 2. Comparison of secondary and tertiary structural properties of HtrA3 and its variants.

(**A**,**B**) Far UV CD between 260 and 195 nm of (**A**) mature HtrA3 (WT in solid circles), Δ134 HtrA3 (del 134 in open circles) and (**B**) HtrA3 SPD (triangles), HtrA3 PDZ (circles), HtrA3 F142D (squares), HtrA3 S305A (diamond) at 25°C with 20 μM of each protein. (**C**,**D**) Fluorescence emission spectra for HtrA3 and its active site mutant with excitation at 295 nm and emission between 310 and 400 nm. Comparison of emission maxima for (**C**) mature HtrA3 (WT, emission max. 342 nm) and HtrA3 S305A (emission max. 342 nm) and (**D**) denatured HtrA3 S305A (solid circles, emission max. 348 nm) and the native protein (open circles, emission max. 342 nm) have been shown. (**E**) Thermal denaturation curves for HtrA3 S305A (open circles) and PDZ (solid circles) within the temperature range of 25–80°C. The CD at 222 nm was selected at each temperature and a plot of fraction folded as a function of temperature is plotted.

steady-state kinetic parameters of $K_{0.5} = 1.04 \pm 0.06$ and $V_{max} = 2.90 \pm 0.26 \times 10^{-13}$ M.s^{-1}. Interestingly, contrary to existing literature [44], on comparison of the kinetic parameters, the V_{max}, k_{cat} and $k_{cat}/K_{0.5}$ of this variant were significantly less compared with the wild-type mature HtrA3 by ~6.7×10^3, 3.6×10^3 and 2.8×10^3 fold,

Table 2 Steady-state kinetic parameters for HtrA3 N-SPD with FITC β-casein as the substrate

Protein	$K_{0.5}$ (μM)	Hill constant	Maximum velocity V_{max} (M.s^{-1})	k_{cat} (s^{-1})	Catalytic efficiency $k_{cat}/K_{0.5}$ (M^{-1} s^{-1})
HtrA3 N-SPD	1.04 ± 0.06	1.53 ± 0.03	$2.90 \pm 0.26 \times 10^{-13}$	$1.53 \pm 0.14 \times 10^{-7}$	0.15 ± 0.02

This data is the average of three independent experiments.

Biochemical Journal (2020) **477** 407–429
https://doi.org/10.1042/BCJ20190706

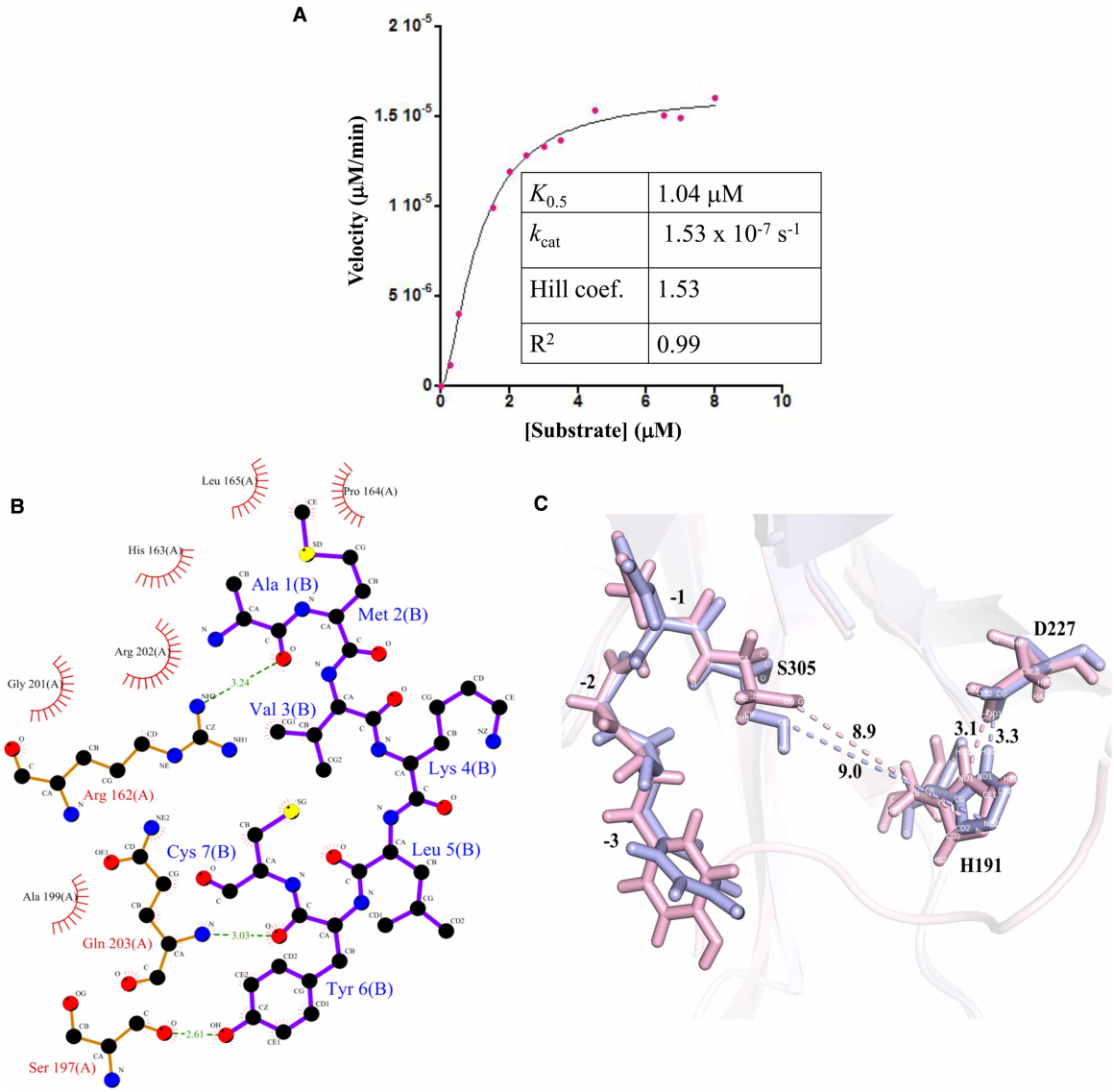

Figure 3. Elucidating the mechanism of catalytic activation in HtrA3 N-SPD.

(**A**) Plot representing the activity and steady-state kinetics of β-casein cleavage by HtrA3 N-SPD. For clarity, SEM values have been mentioned in Table 2. (**B**) Ligplot showing the interacting residues of HtrA3 N-SPD (Chain A) with β-casein (AMVKLYC) peptide (Chain B). Green dotted lines indicate H-bond interactions with distance marked in Å; red semi-circular dashed lines indicate van der Waals interactions. (**C**) Stick diagram showing the alignment of unbound HtrA3 N-SPD (light blue) and peptide-bound N-SPD (pink), representing the oxyanion hole residues along with catalytic residues H191, D227 and S305. Oxyanion hole residues are marked as -1, -2 and -3 starting from the S305 residue which is considered as 0. Distances among the catalytic residues are represented by dashed lines (light blue for unbound and pink for bound HtrA3 N-SPD).

respectively (for mature HtrA3 $V_{max} = 1.95 \pm 0.20 \times 10^{-9}$ M.s^{-1}, $k_{cat} = 0.56 \pm 0.07 \times 10^{-3}$ s^{-1} and $k_{cat}/K_{0.5} = 0.42 \pm 0.03 \times 10^{3}$ $M^{-1}.s^{-1}$) [18]. However, the K_m was slightly decreased by 1.2-fold (for mature HtrA3 $K_{0.5} = 1.31 \pm 0.06$). The drastic decrease in maximum velocity, substrate turnover rates and enzyme catalysis hints toward the presence of a malformed oxyanion hole. Additionally, since the active site pocket is buried 33 Å above the base of the pyramid in the trimeric architecture and β-casein is a C-terminal binding substrate, the deletion of PDZ domain possibly provides greater accessibility to the active site. This, in turn, is reflected in the slight increase in substrate affinity for this variant. Additionally, we reported that the cleavage of β-casein by HtrA3 N-SPD follows a sigmoidal curve with a Hill coefficient of 1.53 ± 0.03 that is less than that of the mature HtrA3 [17].

Biochemical Journal (2020) 477 407–429
https://doi.org/10.1042/BCJ20190706

The absence of PDZ in this variant might lead to greater accessibility of the substrate to the active site; however, it also results in significant decrease in the catalytic efficiency, which might be due to a malformed oxyanion hole as observed previously in the case of its homolog HtrA2 [14].

Therefore, to understand the formation of the oxyanion hole upon β-casein binding, the β-casein peptide (AMVKLYC) [18] was docked with HtrA3 N-SPD at the allosteric site identified in our previous study [18]. Since some of the PDZ domain residues belonging to the allosteric pocket are missing in HtrA3 N-SPD, it resulted in a low docking score of −5.194 kcal/mole (Figure 3B). Moreover, the comparative molecular dynamics (MD) simulation study of the unbound and bound HtrA3 N-SPD showed no significant reorientation of the oxyanion hole residues to form a pocket conducive for substrate cleavage (Figure 3C). These observations provide a solid basis for the decrease in catalytic efficiency for this HtrA3 variant. Furthermore, an exhibition of residual allostery in this ΔPDZ variant might be due to the binding of the β-casein peptide to a part of the allosteric pocket encompassing the residues in the SPD domain (Figure 3B).

Role of N-terminal region and the PDZ domain in oligomerization

HtrAs have a distinctive ability to assemble into complex oligomers [3,55]. This characteristic property of HtrA proteins, along with subtle allosteric modulation often forms the basis of their regulatory mechanisms. While almost all HtrAs share the same basic oligomerization unit of homotrimers (e.g. DegS, HtrA2), some of them assemble into higher-order oligomers comprising 12–24 subunits (e.g. DegQ, DegP). Size exclusion chromatography was performed to understand the role of individual domains as well as critical residues in maintaining the trimeric architecture of HtrA3. The data demonstrate that HtrA3 wild type and active site mutant (S305A) with intact N-terminal region form trimers. PDZ domain alone also formed trimers according to our observation. The predicted molecular mass and oligomerization status of the proteins are shown in Table 3, while representative elution profiles of the HtrA3 variants have been illustrated in Supplementary Figure S1. HtrA3 PDZ is already known to exist as dimers [56]; however, our *in silico* protein–protein docking analysis using PIPER (Bioluminate, Schrödinger, LLC, New York, NY, 2018) shows that three subunits of PDZ domain assemble together to form a trimeric structure. In our study, a total of 10 000 conformations of trimeric assemblies were generated which were further subjected to clustering analysis. Out of 53 generated clusters, the cluster that contained the highest number of conformations was selected as the energetically most favorable trimeric structure. Interaction analysis of this trimeric assembly demonstrates that N-terminal residues such as S351, H352, K354, F356, R360 and M361 as well as C-terminal residues including E450, G456, G458, R459, W460 and V461 from all the three chains form intramolecular H-bonds, van der Waals and salt bridge interactions (Supplementary Figure S2). Apart from N- and C-terminal residues, V391, P393 and Q398 are some of the common interacting residues predominantly forming H-bonds and van der Waal's interactions (Supplementary Figure S2).

HtrA3 N-SPD, HtrA3 SPD–PDZ, HtrA3 F142D and HtrA3 F255D are monomers according to our data. HtrA3 F142A exists as a mixed population of trimers (∼30%) and monomers (∼70%) indicating that the weak interaction between the trimers due to the mutation might lead them to dissociate. Surprisingly, HtrA3 N-SPD variant, despite its intact N-terminal region is a monomer. This hints towards the role of the PDZ domain in oligomerization. The retention volumes (V_e) and predicted molecular mass of HtrA3 SPD alone and Δ143 HtrA3 variant could not be calculated because these proteins aggregated at higher concentrations. Therefore,

Table 3 Oligomeric properties of HtrA3 and its variants

Protein	Theoretical molecular mass (kDa) of single chain	Calculated molecular mass (kDa)	Oligomeric status
HtrA3 wild type (130–453)	36.2	110.2	Trimer
HtrA3 S305A	36.2	101.3	Trimer
HtrA3 PDZ	11.6	33.4	Trimer
HtrA3 F255D and HtrA3 F142D	36.2	42.3	Monomer
HtrA3 SPD–PDZ	31.0	23.3	Monomer

Molecular mass were calculated using Superdex 200 gel filtration column.

contrary to existing report [17], which highlighted the role of F142 residue alone in oligomerization, these results point towards the combinatorial effect of the 'triple lock' (F140, 142, 255), comprising residues from the N-terminus and SPD as well as the PDZ domain in maintaining protein stability and consequently the oligomeric ensemble of HtrA3. The 'triple lock' residues are held tightly together by van der Waals interactions, therefore, mutation of any of these residues leads to disruption of the interaction network which is followed by falling apart of the trimeric organization.

Moreover, the ΔPDZ and Δ143 variants of HtrA3 were found to be very unstable as observed in the thermal denaturation studies, which reiterate the concerted role of the N-terminus and the PDZ in maintaining homotrimerization of HtrA3.

Role of oligomerization, individual domains and critical residues in protease activity

To understand the role of different domains and critical residues in regulating protease activity of HtrA3, its variants and mutants were studied using a generic serine protease substrate β-casein (Figure 4A). These studies along with our observations regarding the oligomerization properties of HtrA3 and variants have been aimed at reflecting protease activity as a consequence of structural/conformational changes due to initial substrate binding.

To characterize substrate catalysis for all these variants and mutants, protease activity was monitored over a time period of 2 h (Figure 4A–E) as well as with increasing concentrations (2–10 μg) of the substrate (Supplementary Figure S3). It was observed that mature HtrA3, its variants (Δ134 HtrA3, Δ143 HtrA3) as well as HtrA3 N-SPD cleaved β-casein but HtrA3 F142D, HtrA3 F142A, HtrA3 F255D, HtrA3 SPD, HtrA3 SPD–PDZ were completely inactive or showed minimal activity even at high substrate concentrations highlighting the importance of the N-terminal region comprising critical 'triple lock' residues in trimerization and hence in HtrA3 activity (Figure 4A). Mature HtrA3 and Δ134 HtrA3 had comparable activity suggesting the deletion did not affect the active site conformation of the protease. Additionally, Δ143 HtrA3 and HtrA3 N-SPD exhibited activity much less than the wild type. These observations suggest that HtrA3 N-SPD, lacking the PDZ domain has a less catalytically competent active site hinting at the role of inter-domain PDZ-protease cross-talk in HtrA3 activation. It also highlights the role of HtrA3 PDZ in mediating conformational changes that aid the formation of a competent active site, which positively influences the rate of catalysis. The substantial decrease in the activity of Δ143 HtrA3 variant, which lacks the F140 and F142 residues that are a part of the 'triple lock', further substantiates the critical role of these phenylalanine residues in maintaining structural integrity, and consequently optimal catalytic activation of HtrA3. Collectively, this emphasizes the role of the N-terminal region as well as the PDZ domain in formation of proper active site conformation and stabilizing the enzyme–substrate complex for catalysis. In the rest of the mutants, though no significant change in enzyme activity was observed, increasing concentrations of substrate showed residual protease activity suggesting that with increase in β-casein concentration, enzyme–substrate complex is more stabilized leading to residual substrate catalysis in these variants. These data emphasize the role of the N-terminus and critical N-terminal residues in protein activity and demonstrates that removal of the PDZ impairs stability, oligomerization (confirmed by size exclusion and thermal denaturation studies) as well as the allosteric protease activation in HtrA3. This also highlights the role of PDZ in substrate catalysis and turnover rate. Thus, it reiterates the requirement of a complex yet precisely co-ordinated intra- and inter-molecular teamwork of different domains of the trimeric protease to perpetuate its activity.

For quantitative analysis, kinetic parameters for mature HtrA3 [18] and HtrA3 N-SPD were determined and our observations have been described in depth in the previous sections. HtrA3 SPD, HtrA3 F142D, HtrA3 F142A, HtrA3 F255D and HtrA3 SPD–PDZ were completely inactive hence no kinetic parameters could be obtained.

Comparative analysis of the structural stability of wild-type HtrA3 and its mutants using MD simulation studies

To understand the roles of amino acid residues F142 and F255 in HtrA3 trimerization, HtrA3 mutants were generated by replacing these residues with aspartic acid in the available crystal structure (model preparation and system generation for MD simulation are discussed in the method section in details) [44]. Structural stability of mature HtrA3, HtrA3 F142D and HtrA3 F255D proteins were monitored with the help of RMSD plot

Biochemical Journal (2020) **477** 407–429
https://doi.org/10.1042/BCJ20190706

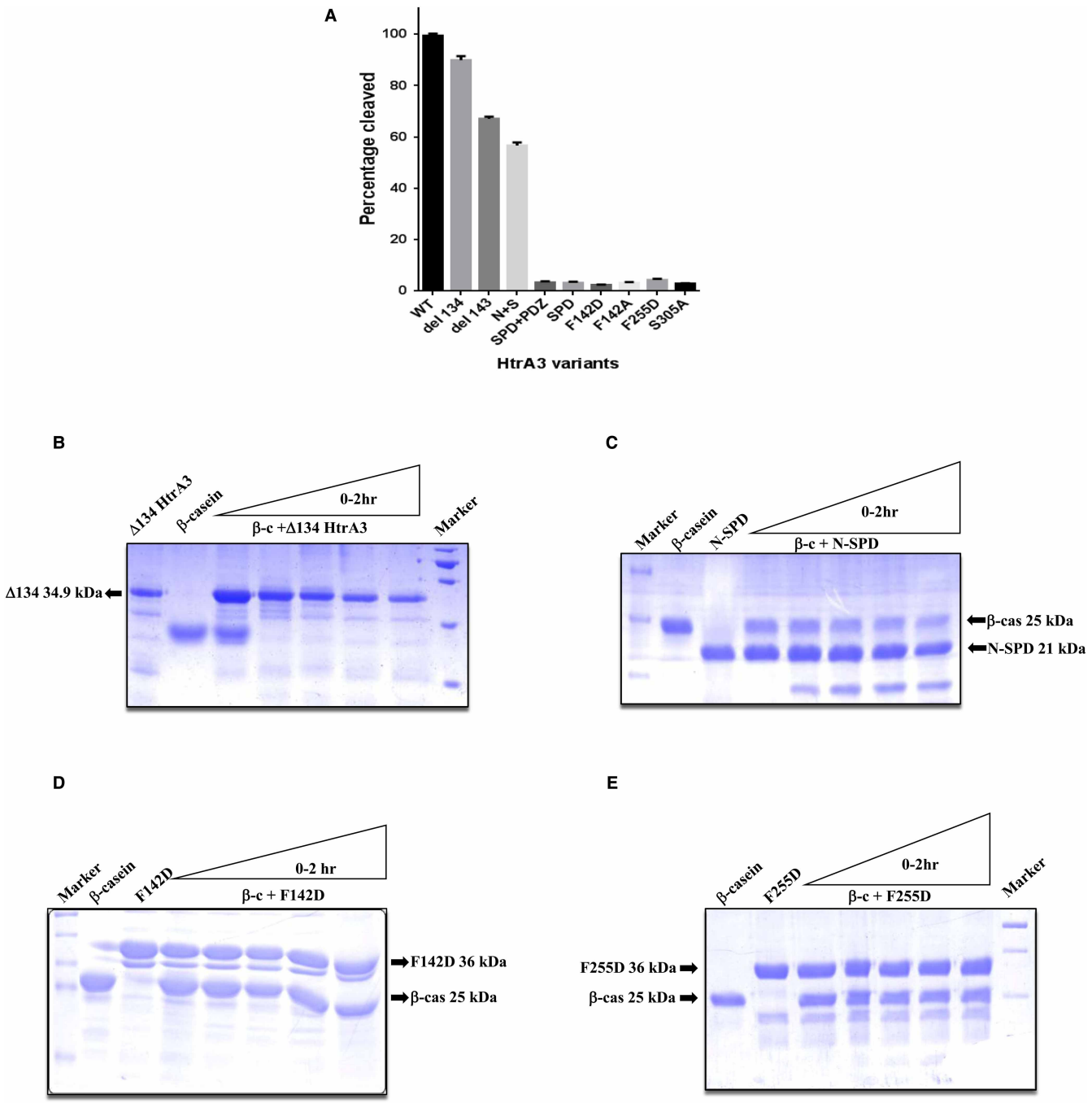

Figure 4. Comparative analysis of proteolytic activities of HtrA3 and its variants with β-casein as a substrate.

(**A**) Plot representing the percentage of β-casein cleaved by different constructs of HtrA3. Respective enzymes were incubated with 6 μg of β-casein at 37°C for 2 h. Reaction samples were resolved by SDS–PAGE and visualized with coomassie brilliant blue staining. The intensity of the substrate remaining after 2 h was semi-quantified using Image J. (The error bars are the representations of SE, $n = 3$). (**B–E**) Representative gel-based β-casein (β-c/β-cas) cleavage assays over a period of 2 h at 37°C with HtrA3 variants, namely, (**B**) Δ134 HtrA3, (**C**) HtrA3 N-SPD, (**D**) HtrA3 F142D and (**E**) HtrA3 F255D. Enzyme and β-casein only used as controls for each assay were also incubated for 2 h at 37°C.

(Figure 5A). Using the HtrA3 crystal structure as the starting reference (PDB ID: **4RI0**), RMSD values of all the atoms in each system were calculated over a period of 100 ns. The plot demonstrated that HtrA3 wild type and its mutant systems converged at ∼18 ns. However, beyond which the RMSD values for the wild type slowly

Biochemical Journal (2020) **477** 407–429
https://doi.org/10.1042/BCJ20190706

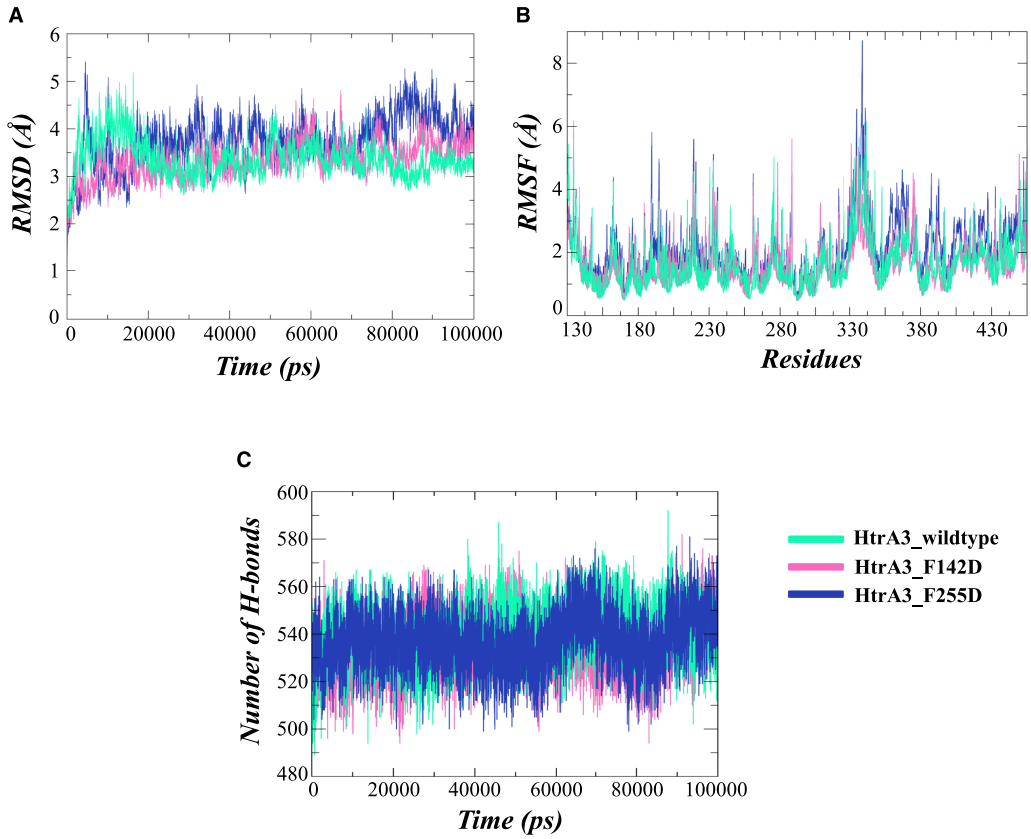

Figure 5. *In silico* comparison of the stability of HtrA3 mutants and the wild-type structures.
Structures of HtrA3 wild type (green), HtrA3 F142D (pink) and HtrA3 F255D (blue) were analyzed using (**A**) Root mean squared deviation (RMSD) plot where the trajectories throughout 100 ns MD simulation represent structural perturbations; (**B**) Root mean squared fluctuation (RMSF) plot indicating structural fluctuation of each residue; (**C**) Hydrogen-bond plot where the changes in the total number of hydrogen bonds throughout the 100 ns MD simulation are represented.

decreased to a stable level of trajectories as compared with the mutants. HtrA3 F255D exhibited the highest deviation from the starting structure, followed by HtrA3 F142D as the trajectories reached near 100 ns (Figure 5A). The mean values of RMSD for mature HtrA3, HtrA3 F142D and HtrA3 F255D were 3.2, 3.7 and 4.8 Å, respectively, indicating greater conformational changes in the mutant proteins, especially F255D, which exhibited a cumulative deviation of 1.6 Å from the wild type. The compactness of these structures was elucidated by the radius of gyration values plotted against their respective RMSD values in the FEL diagrams (Supplementary Figure S4). FELs depicted that the lowest energy conformers for mature HtrA3, HtrA3 F142D and HtrA3 F255D have radius of gyration values of 29.2, 31.1 and 32.8 Å (Supplementary Figures S4A, S4B and S4C), respectively. Lower RMSD and radius of gyration values of the wild type as compared with the mutants further emphasized that mature HtrA3 has a more condensed structure, and intrinsic perturbations in HtrA3 F142D and HtrA3 F255D mutants might be responsible for lesser stable structures [57].

As the convergence of the three systems occurred at 18 ns, the RMSF plots for their residues were generated taking trajectories between 18 and 100 ns into consideration. For the simplified representation of RMSF data, residue-wise RMSF values for one chain (in this case, chain A) have been plotted. Critical analysis of the plot demonstrated higher fluctuations in various loop regions of the mutant proteins (Figure 5B). The highest fluctuation was observed in the linker region (residues 341–359) of HtrA3 F255D mutant which deviated from mature HtrA3 by ∼2 Å (Figure 5B). The time-based plot of the secondary structure evolution further implicated increase in the number of disordered regions (predominantly coils and beta turns) in HtrA3 F255D and HtrA3 F142D with respect to the wild type in Supplementary Figure S5. In addition, when the number of intramolecular hydrogen bonds (H-bonds) was calculated using filtering parameters such as distance (cut-off value of 3.5 Å) and angle (cut-off value of 35°), a decrease in values was observed. The mean H-bond count

Biochemical Journal (2020) **477** 407–429
https://doi.org/10.1042/BCJ20190706

decreased from 542 (in mature HtrA3) to 527 (in HtrA3 F142D) and 521 (in HtrA3 F255D), respectively (Figure 5C) [58].

Cα atomic distance analysis of the catalytic triad residues

Distances among Cα atoms of H191, D227 and S305, which encompass the HtrA3 catalytic pocket were calculated at 2 fs intervals and plotted against 100 ns of MD simulation run for all the three systems to understand the effect of mutations in HtrA3 catalytic activity (Figure 6) [17]. For a proper catalytic pocket formation in serine proteases, histidine usually moves closer to aspartate while serine moves away from the histidine residue [1,12]. This results in an open conformation that is sufficient for accommodating substrate molecules as well as maintaining an optimum distance between histidine and serine to facilitate the formation of a metastable tetrahedral intermediate (active form), resulting from the histidine-induced deprotonation of serine residue [1,12]. However, in the case of HtrA3 F142D and HtrA3 F255D, the average distance between H191 and D227 in all the three chains increased within a range of 0.6–1.1 Å when compared with the mature HtrA3 (Figure 6A,C,E). Similarly, a drastic decrease within range of 1.2–3.8 Å was observed when the average distance between H191

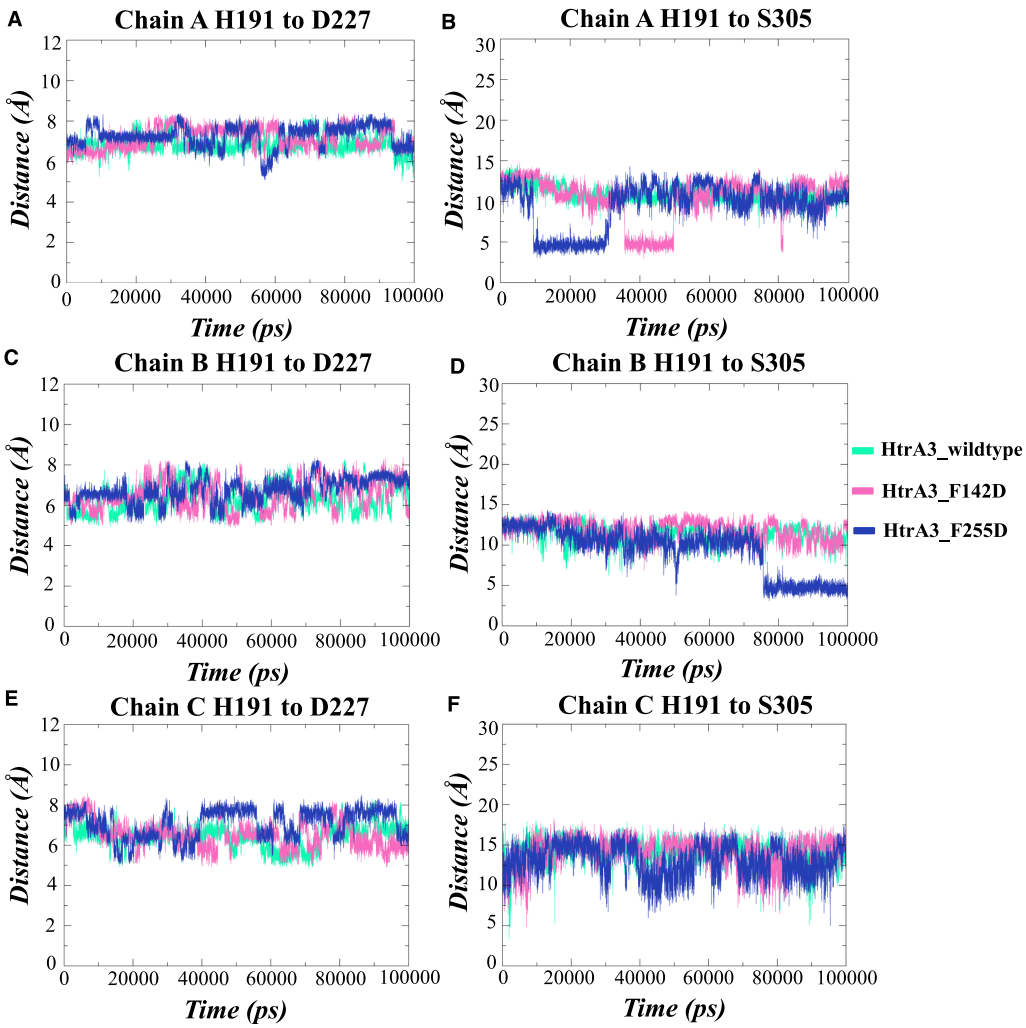

Figure 6. Comparative analysis of the distances between the catalytic triad residues for HtrA3 and its mutants.

Distance analysis plots showing 100 ns trajectories representing the changes in the distance between H191and D227 in (**A**) chain A; (**C**) chain B; and (**E**) chain C, respectively, as well as distance between H191 and S305 in (**B**) chain A; (**D**) chain B and (**F**) chain C, respectively. Color representation for HtrA3 and its mutants are: HtrA3 wild type in green, HtrA3 F142D in pink and HtrA3 F255D in blue.

and S305 was compared with mature HtrA3 (Figure 6B,D,F). These movements resulted in a closed active site pocket where the relative orientation of the catalytic triad is not conducive of maintaining optimal HtrA3 activity. This analysis further explains the inactivity of F142D and F255D variants of HtrA3 where the catalytic activity is substantially reduced due to disordered catalytic pocket formation.

Role of temperature in protease activity

Among human HtrAs, HtrA2 in particular, shows a significant increase in activity with temperature [13,14]. This heat activation is associated with considerable plasticity at the PDZ-protease interface similar to activation via substrate binding at PDZ [12,14]. We speculated that HtrA3 might also exhibit similar changes in activity as a function of temperature. Therefore, protease assays of HtrA3 were performed where HtrA3 variants were incubated with 6 μg of β-casein in the temperature range of 30–60°C for 10 and 30 min. The proteolytic products were then analyzed using SDS–PAGE gels. We observed that HtrA3 completely processes substrate at all temperatures except at 30°C when incubated for 10 min (Figure 7A,B). These results are also supported by both quantitative enzyme kinetics studies as well as gel-based assays described in the previous sections. However, with subsequent increase in temperature beyond 50°C, we observed significant degradation of HtrA3, which might be due to protease destabilization as also observed by thermal denaturation studies (Figure 7C). Overall, for HtrA3, rise in temperature above 30°C might induce the necessary conformational changes required for efficient proteolytic activity. However, for temperatures above 50°C, catalysis is also accompanied by protein degradation that might be a consequence of protease destabilization.

Htra3 cleaves β-casein at four specific sites

To determine the cleavage specificity of HtrA3 and to investigate if it shares a similar specificity profile with its other human counterparts, namely HtrA1 and HtrA2, proteolytic studies were performed using β-casein as the

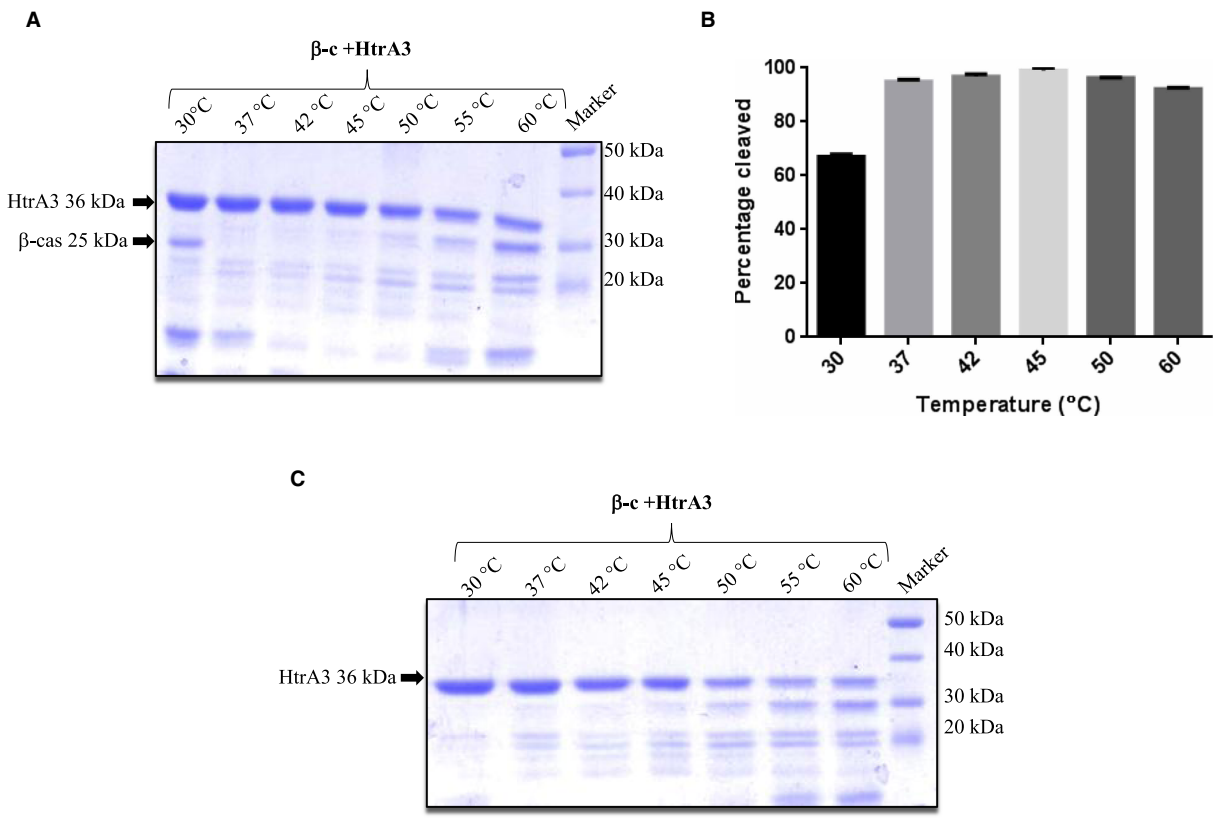

Figure 7. Proteolytic activity of mature HtrA3 as a function of temperature (30–60°C) using β-casein as substrate.

(**A** and **C**) Gel-based β-casein (β-c/β-cas) cleavage assays over 30–60°C, where reactions were incubated for 10 and 30 min, respectively. (**B**) The plot of proteolytic activities of HtrA3 over 30–60°C has been semi-quantified using Image J.

Biochemical Journal (2020) **477** 407–429
https://doi.org/10.1042/BCJ20190706

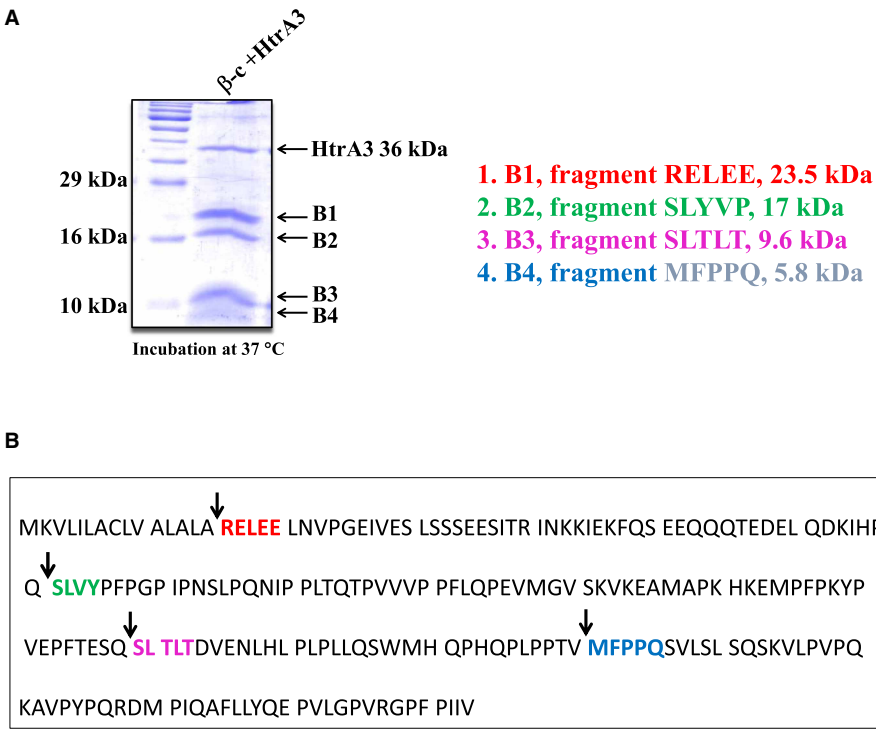

Figure 8. Substrate specificity of HtrA3.

(**A**) Protease assay of HtrA3 with substrate β-casein peptide fragments B1–B4 were excised and sent for N-terminal sequencing. (**B**) Identified cleavage sites are highlighted in red, green, pink and blue, respectively. The four cleavage sites are also indicated by black arrows.

substrate. Proteolytically cleaved fragments were resolved on SDS–PAGE gel and four cleaved fragments (between ∼5 and 24 kDa) of β-casein were isolated (Figure 8A). These fragments were further subjected to N-terminal sequencing by Edman degradation. Upon analysis of these fragments, four preferred cleavage sites on β-casein were identified (Figure 8B). The cleavage sites from first to fourth are between 15A-16R, 71Q-72S, 138Q-139S and 170V-171M amino acids, respectively. The specificity profile of the four sites has been highlighted in Table 4.

Our observations suggest that HtrA3, similar to the other human HtrA homologs, has a strong preference for aliphatic residues at P1 (A, V and Q) position (Table 5). At the P2 position, aliphatic (L) and polar (S, T) residues are preferred, again similar to HtrA1 and HtrA2 (L). P3 and P4 positions are occupied by aliphatic (L, A), polar residues (T, Q), nonpolar (P) and acidic (E) residues, which also matches with that of HtrA1 and 2 (A, L, P, Q). For the P1′ positions, we observed that HtrA3 preferred aliphatic (M) and polar amino acids (S, R), similar to other family members. While, P2′ position was occupied by acidic (E), aromatic (F) and aliphatic

Table 4 Substrate specificity of HtrA3

	P4	P3	P2	P1		P1′	P2′	P3′	P4′	P1′ residue
Site 1	L	A	L	A	—	R	E	L	E	Arg 16
Site 2	A	Q	T	Q	—	S	L	V	Y	Ser 72
Site 3	T	E	S	Q	—	S	L	T	L	Ser 139
Site 4	P	P	T	V	—	M	F	P	P	Met 171

Sites1–4 are the four sites of cleavage that were identified. Prime (P) and nonprime (P′) residues at these sites have been identified through N-terminal sequencing.

Biochemical Journal (2020) 477 407–429
https://doi.org/10.1042/BCJ20190706

Table 5 Substrate specificity of HtrA family members [63–65]

Position	HtrA1	HtrA2	HtrA3	HtrA4
P1	A,M,I,V,L	M,I,V	A,Q,Q,V	A,M,V
P2	L,T	L,R	L,T,S,T	L,V,T
P3	Q,L	K,R,Y	A,Q,E,P	E,A,P
P4	A,P	L,P,I	L,A,T,P	L,P
P1′	R,S,T	S,A	R,S,S,M	R,G,M
P2′	L,P,W	Y,F	E,L,L,F	E,V,F
P3′	V,M,D	S,P,Y	L,V,T,P	S,P,L
P4′	F	F,Y,S	E,Y,L,P	E,K,P

(L) residues, P3′ position had aliphatic (L, V), polar (T) as well as nonpolar (P) residues. At P4′, HtrA3 showed a preference for aliphatic (L), aromatic (Y), nonpolar (P) and acidic (E) residues. Comparatively, HtrA1 and HtrA2 showed preference for similar residues at P1–P4 and P1′–P4′ sites suggesting that they have similar (but not identical) substrate specificities (Table 5).

Discussion

The aim of this study was to gain an in-depth knowledge as well as to re-examine existing hypotheses on the structure–function relationship, mode of activation and specificity of HtrA3. We delineated the role of different domains and their combinations, critical residues and oligomerization in modulating HtrA3 activity and specificity with an aim at developing a working model for the activation mechanism of HtrA3.

For many proteases of the HtrA family, allosteric mode of regulation is a well-known mechanism of catalytic activation. In the bacterial HtrAs such as DegS, DegP and DegQ, it is well documented that their active site pockets get allosterically stabilized or activated by substrate binding at the distal regulatory PDZ domain [59]. For the human HtrAs, an allosteric mode of activation is well established in the literature for all human HtrAs (-1,-2 and -4) except HtrA3 [12,13]. We recently demonstrated that an allosteric mode of regulation exists for HtrA3 through a novel non-canonical pocket spanning residues both in the SPD and PDZ domains [18]. Moreover, this extended binding patch does not include any major residue from the conserved binding groove *aka* GLGF motif (here FIGI) in PDZ domain, which is unique in this protease [18]. It has been observed that peptide binding to the allosteric site causes movements in the regulatory loops LD, L1 and LA that eventually lead to a catalytically favorable active site formation [18]. This is especially interesting since it opens up avenues for easily and efficiently manipulating the protease activity of HtrA3.

Interestingly, in the present study, the ΔPDZ variant (HtrA3 N-SPD), which also demonstrates allosteric propagation with positive Hill coefficient has very less activity. This although seems counter-intuitive, could be well explained by the absence of oxyanion hole reorientation that occurs as a consequence of inter-domain PDZ-protease cross-talk as demonstrated by enzyme kinetic and MD simulation studies. Moreover, the residual positive allostery observed in HtrA3 N-SPD can be attributed to the amino acids in SPD domain that contribute to the non-canonical allosteric pocket [18]. Therefore, contrary to a previous report [17], which proposes the dispensability of PDZ in HtrA3 activity, our findings underscore the requirement of PDZ in efficient allosteric propagation and overall activity of HtrA3 thus redefining its mechanism of action. In addition, its well-studied homolog, HtrA2, also exhibits a similar mode of activity [12,14,16]. Besides, there are reports that demonstrate that exogenous full-length HtrA3 is more efficient than its PDZ-lacking variant in inducing apoptosis in cancer cells [41].

Human HtrAs are primarily trimeric [13,14] while their prokaryotic counterparts are capable of forming higher-order oligomers [3]. HtrA3 crystal structure represents a trimeric ensemble of three molecules of the monomeric protein where three phenylalanine residues (F140, F142 and F255) from each monomeric chain 'lock' together to stabilize the trimer. These amino acids belong to two conserved regions of homo-trimerization in human HtrAs as defined in earlier literature reports [44]. In HtrA3, the first region (K**F**N**F**IADVVEK, amino acids 139–149) encompasses F140 and F142 residues, while the second region (LRPGE**F**VVAIGSPFALQ, amino acids 250–266) harbors residue F255. Our studies using these critical phenylalanine single mutants (HtrA3 F142D, HtrA3 F142A and HtrA3 F255D) showed that these mutations render

Biochemical Journal (2020) **477** 407–429
https://doi.org/10.1042/BCJ20190706

the proteins inactive and monomeric. In the case of Δ143 HtrA3 (lacking F140) deletion variant, destabilization of the protein was observed in both thermal denaturation and size exclusion chromatography studies, which might be responsible for a drastic decrease in the activity of this variant (as observed in enzymatic studies). Additionally, our *in silico* MD simulation study demonstrated higher RMSD and radius of gyration (Rg) values, along with loss of intramolecular hydrogen bonds for HtrA3 F142D and HtrA3 F255D mutants, when compared with mature HtrA3. This further explains the less stable structures and higher intrinsic perturbations in the mutants [57]. Apart from structural instability, malformation of the catalytic pocket was also observed in the mutant systems where the catalytic triad residues (H191, D227 and S305) show movements, which are not conducive towards the formation of proper catalytically active conformation [1]. These results collectively substantiate the fact that 'triple-lock' residues such as F142 and F255 are critical in maintaining structural integrity and catalytic activity of HtrA3 protein. Apart from this, we showed that while mature HtrA3 (wild type), HtrA3 S305A and HtrA3 PDZ tend to form trimers, HtrA3 SPD–PDZ and HtrA3 N-SPD are completely monomeric. These observations unambiguously demonstrate for the first time that the N-terminal region, PDZ domain and the 'triple lock' residues all contribute in a co-ordinated manner towards homo-trimerization, stability and hence the formation of a functional trimeric ensemble of the protease.

The N-terminal trimerization region and the C-terminal PDZ domain in HtrA homologs are known to perform a myriad of functions including IAP binding, active site rearrangement, stabilization of enzyme–substrate complex, allosteric modulation, protein–protein interactions and oligomerization [60]. In HtrA2, the N-terminal region plays an important role in active site rearrangement and providing stability to the protein, while the PDZ is involved in substrate binding via the YIGV tetrapeptide (GLGF motif) and regulating the activity of the protein, among other functions [16]. Through our gel-based enzyme assays with HtrA3 mutants and variants, we affirmed that proteins lacking the N-terminal region (HtrA3 SPD–PDZ) or both PDZ and N-terminal region (HtrA3 SPD) or any of the critical phenylalanine residues (HtrA3 F142D, HtrA3 F142A and HtrA3 F255D) are completely inactive. Constructs without certain N-terminal elements or the PDZ domain, exhibited a drastic loss in their enzymatic activity (Δ143 HtrA3 and HtrA3 N-SPD, respectively). These observations unambiguously suggest that N-terminal region plays an important role in regulating its activity. Hereby, we also challenged the existing hypothesis that PDZ might be dispensable for optimal catalytic activity [17] and proved its critical role in allosteric activation of the protease.

The known physiological substrates of HtrA3 are limited, most of which include proteoglycans [23,24], XIAP and a few cytoskeletal proteins [61,62]. These interactions suggest that HtrA3 functions are regulated by complex multiple pathways involving its protease activity and the mechanisms of substrate specificity and cleavage may, therefore, play a significant role. Hence, we examined the cleavage specificity of the HtrA3 protease using β-casein as substrate. The study revealed three additional unique cleavage sites apart from those reported in the literature [17]. HtrA3 showed a preference for similar residues at P1–P4 and P1′–P4′ sites when compared with HtrA1 and HtrA2 [63–65], suggesting that they have similar but not identical substrate specificities that might be important for its specific cellular activities. Additionally, we investigated the effects of temperature on HtrA3 mediated substrate cleavage and concluded that it exhibits an increase in activity with temperature similar to its homologs [14,66]. Activity studies suggested that HtrA3 activity increased beyond 30°C and was accompanied by destabilization of the protein post 50°C, which was also reflected in our stability studies. This might point towards additional roles of HtrA3 in protein quality control under cellular stress conditions such as heat shock which is a primary function in its homologs, especially HtrA2 [66]. HtrA3, with a melting temperature of 63°C has more stability compared with HtrA4 (58°C) but less than that of HtrA2 (73°C) [13,14] suggesting that the conformational changes induced in these proteins by temperature might be different.

Therefore, besides ascertaining the contribution of domains and residues in HtrA3 structure and function, we also re-evaluated and provided a comprehensive illustration of the mode of HtrA3 activation as shown in Figure 9. *For the first time*, we have underlined the roles of both the N-terminus and the PDZ in holding the structure in a stable oligomeric ensemble and proper active site formation. This is also validated by the fact that HtrA3 N-SPD and HtrA3 SPD–PDZ are both monomers. Besides, thermal denaturation studies demonstrate that removal of the PDZ leads to a decrease in protein stability which might be because the PDZ of each chain interacts and stabilizes the LB loop region of SPD as well as the hinge region between the two domains. The critical hotspots of these interactions have been highlighted by the dotted surface in Figure 9A (inset). Previous reports suggest that residues N196, S197, A198, A199, G201 of the LB loop might interact with H6 helix region (E371) and β15 strand region (Q389) of the PDZ domain [18,32]. Moreover, the interaction of the PDZ with

Biochemical Journal (2020) **477** 407–429
https://doi.org/10.1042/BCJ20190706

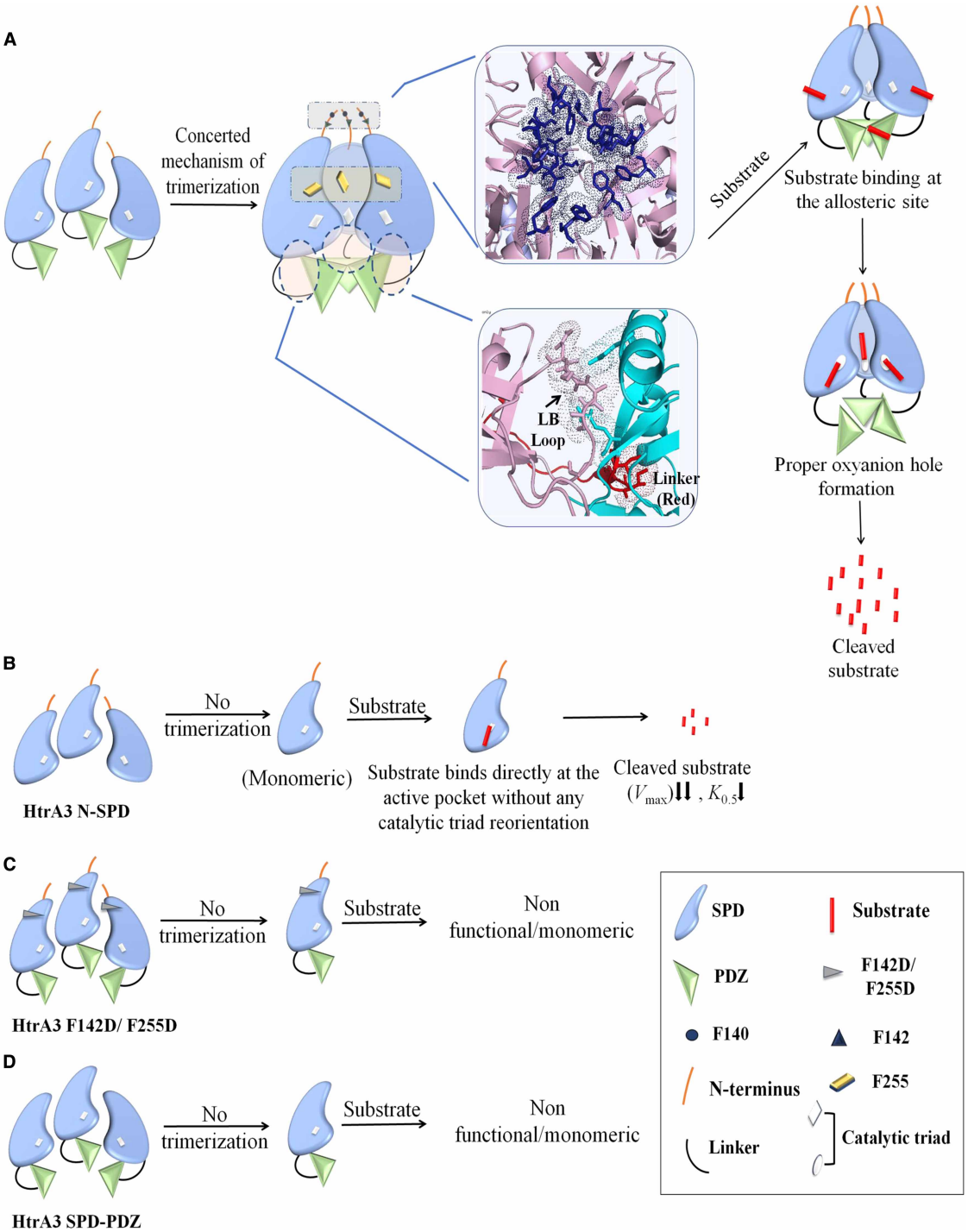

Figure 9. Model for the mechanism of HtrA3 activation. Part 1 of 2

(**A**) In mature HtrA3, the individual chains of the protein are held together in a trimeric ensemble by the N-terminus, a residue from SPD and the PDZ domain in a co-ordinated manner (interacting surfaces are shown as dotted circles and residues in stick models). Substrate binding at the allosteric site triggers a cascade of events that lead to reorientations of the catalytic triad residues along with the formation of a functional oxyanion hole, which makes the protease well poised for further substrate binding and catalysis. (**B**) In monomeric HtrA3 N-SPD, the absence of PDZ allows easy access of substrate to the active site which leads to an increase in substrate affinity; however, lack of reorientations at the catalytic triad due to inability to form a functional trimer leads to a drastic decrease in activity. (**C**) Monomeric 'phenylalanine lock' variants HtrA3 F142D and HtrA3

Biochemical Journal (2020) **477** 407–429
https://doi.org/10.1042/BCJ20190706

Figure 9. Model for the mechanism of HtrA3 activation. Part 2 of 2

F255D with malformed active site make these variants non-functional. (**D**) Monomeric HtrA3 SPD–PDZ with the malformed active site makes this variant non-functional.

the hinge region at the PDZ-protease interface might be mediated through P449 and I359. We have also shown that the PDZ domain alone forms a stable trimer, which is unique among HtrAs.

Multiple members of the human HtrA proteases promote apoptosis exhibiting functional redundancy within the family. We speculate that the synergistic dual control of the N-terminal region and PDZ on proper structural assembly and activity offers a tighter control on HtrA3's apoptotic functions, which might be important for maintaining cellular homeostasis. Moreover, the protease is also involved in embryo implantation and development of the placenta [67]. It is known that defects in adequate trophoblast invasion results in poor maternal-fetal circulation and placental hypoxia, while excessive invasion into the endometrium is associated with invasive choriocarcinoma. Therefore, the invasion of the interstitial extravillous trophoblast cells (EVTs) is tightly regulated to ensure a successful pregnancy [68]. Decidua-secreted HtrA3 has been found to negatively regulate trophoblast migration and invasion that is critical for a healthy pregnancy. HtrA3 has been implied in inhibiting TGF-β (transforming growth factor beta) signaling—an important regulator of pro- and antiangiogenic balance during fetal development. High levels of HtrA3 hence leads to pathogenesis of pre-eclampsia that is a major cause of pregnancy-related morbidity across the globe. TGF-β signaling is also known to stimulate oncogenesis and a dramatic decrease in HtrA3 level is often observed in many tumors. Literature reports that HtrA3 either inhibits TGF-β through direct protein–protein interactions and/or through proteolytic cleavage of components of the extracellular matrix (ECM). Therefore, this fundamental study on the allosteric mode of HtrA3 activation opens up possibilities of designing appropriate peptidomimetics or small molecule analogs to favorably manipulate HtrA3 functions for disease intervention. For example, allosteric activators of HtrA3 may be used to promote cancer cell apoptosis in certain cancers. Alternatively, new allosteric sites such as the one reported by our group [18] may be used to efficiently regulate the proteolytic activity of this protein in cancers where it is down-regulated. For diseases such as pre-eclampsia, active site-specific inhibitors can be designed based on active site architecture and substrate specificity of this protease. Overall, a complete understanding of the mechanisms underlying HtrA3 functions offers many possibilities towards devising successful therapeutic strategies.

Abbreviations

ADH, alcohol dehydrogenase; BSA, bovine serum albumin; ECM, extra cellular matrix; FITC, fluorescein isothiocyanate; GROMACS, GRoningen MAchine for Chemical Simulation; HtrA, high-temperature requirement protease A; HtrA3, high temperature requirement serine protease A3; IAP, inhibitor of apoptosis; IBM, IAP binding motif; IGFBP, insulin-like growth factor-binding domain; KI, Kazal-like protease-inhibitor domain; LINCS, LINear Constraint Solver; MBP, maltose-binding protein; MD, molecular dynamics; NPT, N = number of particles, P = system's pressure, T = absolute temperature; N-SPD, N-terminal and serine protease domain; NVT, N = number of particles, V = system's volume, T = absolute temperature; PME, particle-mesh Ewald method; RMSD, root mean squared deviation; RMSF, root mean squared fluctuation; SPD, serine protease domain; UPR, unfolded protein response; WT, wild type; XIAP, X-linked inhibitor of apoptosis.

Author Contribution

S.A. and K.B. conceived and designed the study. S.A. and S.D. conducted all the experiments. Data analysis and manuscripts preparation were done by S.A., S.D. and K.B. All authors read and approved the manuscript.

Funding

This work was supported by the Advanced Center for Training Research and Education in Cancer (ACTREC) (Grant No. 3842 and 42). The authors also thank BTIS, ACTREC for providing infrastructure for the necessary experiments.

Acknowledgement

We thank Mriganka Mandal and Sucheta Chopra for helping with protein purification, Late Dr. Lalith K Chaganti for his intellectual inputs.

PORTLAND PRESS

Competing Interests

The authors declare that there are no competing interests associated with the manuscript.

References

1 Singh, N., Kuppili, R.R. and Bose, K. (2011) The structural basis of mode of activation and functional diversity: a case study with HtrA family of serine proteases. *Arch. Biochem. Biophys.* **516**, 85–96 https://doi.org/10.1016/j.abb.2011.10.007
2 Clausen, T., Kaiser, M., Huber, R. and Ehrmann, M. (2011) HTRA proteases: regulated proteolysis in protein quality control. *Nat. Rev. Mol. Cell Biol.* **12**, 152–162 https://doi.org/10.1038/nrm3065
3 Jiang, J., Zhang, X., Chen, Y., Wu, Y., Zhou, Z.H., Chang, Z. et al. (2008) Activation of DegP chaperone–protease via formation of large cage-like oligomers upon binding to substrate proteins. *Proc. Natl Acad. Sci. U.S.A.* **105**, 11939–11944 https://doi.org/10.1073/pnas.0805464105
4 Krojer, T., Garrido-Franco, M., Huber, R., Ehrmann, M. and Clausen, T. (2002) Crystal structure of DegP (HtrA) reveals a new protease-chaperone machine. *Nature* **416**, 455–459 https://doi.org/10.1038/416455a
5 Krojer, T., Sawa, J., Schäfer, E., Saibil, H.R., Ehrmann, M. and Clausen, T. (2008) Structural basis for the regulated protease and chaperone function of DegP. *Nature* **453**, 885–890 https://doi.org/10.1038/nature07004
6 Shen, Q.-T., Bai, X.-C., Chang, L.-F., Wu, Y., Wang, H.-W. and Sui, S.-F. (2009) Bowl-shaped oligomeric structures on membranes as DegP's new functional forms in protein quality control. *Proc. Natl Acad. Sci. U.S.A.* **106**, 4858–4863 https://doi.org/10.1073/pnas.0811780106
7 Wilken, C., Kitzing, K., Kurzbauer, R., Ehrmann, M. and Clausen, T. (2004) Crystal structure of the DegS stress sensor: how a PDZ domain recognizes misfolded protein and activates a protease. *Cell* **117**, 483–494 https://doi.org/10.1016/S0092-8674(04)00454-4
8 Clausen, T., Southan, C. and Ehrmann, M. (2002) The HtrA family of proteases: implications for protein composition and cell fate. *Mol. Cell* **10**, 443–455 https://doi.org/10.1016/S1097-2765(02)00658-5
9 Gray, C.W., Ward, R.V., Karran, E., Turconi, S., Rowles, A., Viglienghi, D. et al. (2000) Characterization of human HtrA2, a novel serine protease involved in the mammalian cellular stress response. *Eur. J. Biochem.* **267**, 5699–5710 https://doi.org/10.1046/j.1432-1327.2000.01589.x
10 Nie, G.-Y., Hampton, A., Li, Y., Findlay, J.K. and Salamonsen, L.A. (2003) Identification and cloning of two isoforms of human high-temperature requirement factor A3 (HtrA3), characterization of its genomic structure and comparison of its tissue distribution with HtrA1 and HtrA2. *Biochem. J.* **371** (Pt 1), 39-48 https://doi.org/10.1042/bj20021569
11 Kim, ,D.Y., Kim, K.K. (2005) Structure and function of HtrA family proteins, the key players in protein quality control. *J. Biochem. Mol. Biol.* **38**, 266–274 https://doi.org/10.5483/bmbrep.2005.38.3.266
12 Bejugam, P.R., Kuppili, R.R., Singh, N., Gadewal, N., Chaganti, L.K., Sastry, G.M. et al. (2013) Allosteric regulation of serine protease HtrA2 through novel non-canonical substrate binding pocket. *PLos One* **8**, e55416-e https://doi.org/10.1371/journal.pone.0055416
13 Kummari, R., Dutta, S., Chaganti, L.K. and Bose, K. (2019) Discerning the mechanism of action of HtrA4: a serine protease implicated in the cell death pathway. *Biochem. J.* **476**, 1445–1463 https://doi.org/10.1042/BCJ20190224
14 Chaganti, L.K., Kuppili, R.R. and Bose, K. (2013) Intricate structural coordination and domain plasticity regulate activity of serine protease HtrA2. *FASEB J.* **27**, 3054–3066 https://doi.org/10.1096/fj.13-227256
15 Eigenbrot, C., Ultsch, M., Lipari Michael, T., Moran, P., Lin, S.J., Ganesan, R. et al. (2012) Structural and functional analysis of HtrA1 and its subdomains. *Structure* **20**, 1040–1050 https://doi.org/10.1016/j.str.2012.03.021
16 Singh, N., D'Souza, A., Cholleti, A., Sastry, G.M. and Bose, K. (2014) Dual regulatory switch confers tighter control on HtrA2 proteolytic activity. *FEBS J.* **281**, 2456–2470 https://doi.org/10.1111/febs.12799
17 Glaza, P., Osipiuk, J., Wenta, T., Zurawa-Janicka, D., Jarzab, M., Lesner, A. et al. (2015) Structural and functional analysis of human HtrA3 protease and its subdomains. *PLos One* **10**, e0131142 https://doi.org/10.1371/journal.pone.0131142
18 Acharya, S., Dutta, S., Chopra, S. and Bose, K. (2019) Identification of a distal allosteric ligand binding pocket in HtrA3. *Biochem. Biophys. Res. Commun.* **516**, 1137–1143 https://doi.org/10.1016/j.bbrc.2019.07.005
19 Oka, C., Tsujimoto, R., Kajikawa, M., Koshiba-Takeuchi, K., Ina, J., Yano, M. et al. (2004) Htra1 serine protease inhibits signaling mediated by Tgfβ family proteins. *Development* **131**, 1041–1053 https://doi.org/10.1242/dev.00999
20 Chien, J., Ota, T., Aletti, G., Shridhar, R., Boccellino, M., Quagliuolo, L. et al. (2009) Serine protease HtrA1 associates with microtubules and inhibits cell migration. *Mol. Cell. Biol.* **29**, 4177–4187 https://doi.org/10.1128/MCB.00035-09
21 Narkiewicz, ,J., Lapinska-Szumczyk, S., Zurawa-Janicka, D., Skorko-Glonek, J., Emerich, J. et al. (2009) Expression of human HtrA1, HtrA2, HtrA3 and TGF-β1 genes in primary endometrial cancer. *Oncol. Rep.* **21**, 1529-1537 https://doi.org/10.3892/or_00000385
22 Beleford, D., Liu, Z., Rattan, R., Quagliuolo, L., Boccellino, M., Baldi, A. et al. (2010) Methylation induced gene silencing of HtrA3 in smoking-related lung cancer. *Clin. Cancer Res.* **16**, 398–409 https://doi.org/10.1158/1078-0432.CCR-09-1677
23 Tocharus, J., Tsuchiya, A., Kajikawa, M., Ueta, Y., Oka, C. and Kawaichi, M. (2004) Developmentally regulated expression of mouse HtrA3 and its role as an inhibitor of TGF-β signaling. *Dev. Growth Differ.* **46**, 257–274 https://doi.org/10.1111/j.1440-169X.2004.00743.x
24 Campioni, M., Severino, A., Manente, L., Tuduce, I.L., Toldo, S., Caraglia, M. et al. (2010) The serine protease HtrA1 specifically interacts and degrades the tuberous sclerosis complex 2 protein. *Mol. Cancer Res.* **8**, 1248–1260 https://doi.org/10.1158/1541-7786.MCR-09-0473
25 Trencia, A., Fiory, F., Maitan, M.A., Vito, P., Barbagallo, A.P.M., Perfetti, A. et al. (2004) Omi/HtrA2 promotes cell death by binding and degrading the anti-apoptotic protein ped/pea-15. *J. Biol. Chem.* **279**, 46566–46572 https://doi.org/10.1074/jbc.M406317200
26 Cilenti, L., Soundarapandian, M.M., Kyriazis, G.A., Stratico, V., Singh, S., Gupta, S. et al. (2004) Regulation of HAX-1 anti-apoptotic protein by Omi/HtrA2 protease during cell death. *J. Biol. Chem.* **279**, 50295–50301 https://doi.org/10.1074/jbc.M406006200
27 Xia, J., Wang, F., Wang, L. and Fan, Q. (2013) Elevated serine protease HtrA1 inhibits cell proliferation, reduces invasion, and induces apoptosis in esophageal squamous cell carcinoma by blocking the nuclear factor-κB signaling pathway. *Tumor Biol.* **34**, 317–328 https://doi.org/10.1007/s13277-012-0553-6
28 Bose, K. (2015). *Proteases in Apoptosis: Pathways, Protocols and Translational Advances*, 1st edn, Springer International Publishing, Switzerland. 245 p.
29 Martins, L.M., Iaccarino, I., Tenev, T., Gschmeissner, S., Totty, N.F., Lemoine, N.R. et al. (2002) The serine protease Omi/HtrA2 regulates apoptosis by binding XIAP through a reaper-like motif. *J. Biol. Chem.* **277**, 439–444 https://doi.org/10.1074/jbc.M109784200

Biochemical Journal (2020) **477** 407–429
https://doi.org/10.1042/BCJ20190706

30 Althaus, J., Siegelin, M.D., Dehghani, F., Cilenti, L., Zervos, A.S. and Rami, A. (2007) The serine protease Omi/HtrA2 is involved in XIAP cleavage and in neuronal cell death following focal cerebral ischemia/reperfusion. *Neurochem. Int.* **50**, 172–180 https://doi.org/10.1016/j.neuint.2006.07.018
31 Suzuki, Y., Imai, Y., Nakayama, H., Takahashi, K., Takio, K. and Takahashi, R. (2001) A serine protease, HtrA2, is released from the mitochondria and interacts with XIAP, inducing cell death. *Mol. Cell.* **8**, 613–621 https://doi.org/10.1016/S1097-2765(01)00341-0
32 Wenta, T., Glaza, P., Jarząb, M., Zarzecka, U., Żurawa-Janicka, D., Lesner, A. et al. (2017) The role of the LB structural loop and its interactions with the PDZ domain of the human HtrA3 protease. *Biochim. Biophys. Acta* **1865**, 1141–1151 https://doi.org/10.1016/j.bbapap.2017.06.013
33 Zurawa-Janicka, D., Skorko-Glonek, J. and Lipinska, B. (2010) Htra proteins as targets in therapy of cancer and other diseases. *Expert Opin. Ther. Targets* **14**, 665–679 https://doi.org/10.1517/14728222.2010.487867
34 Nie, G.Y., Li, Y., Minoura, H., Batten, L., Ooi, G.T., Findlay, J.K. et al. (2003) A novel serine protease of the mammalian HtrA family is up-regulated in mouse uterus coinciding with placentation. *Mol. Hum. Reprod.* **9**, 279–290 https://doi.org/10.1093/molehr/gag036
35 Dynon, K., Heng, S., Puryer, M., Li, Y., Walton, K., Endo, Y. et al. (2012) Htra3 as an early marker for preeclampsia: specific monoclonal antibodies and sensitive high-throughput assays for serum screening. *PLos One* **7**, e45956-e https://doi.org/10.1371/journal.pone.0045956
36 Li, Y., Salamonsen, L.A., Hyett, J., FdS, C. and Nie, G. (2017) Maternal HtrA3 optimizes placental development to influence offspring birth weight and subsequent white fat gain in adulthood. *Sci. Rep.* **7**, 4627 https://doi.org/10.1038/s41598-017-04867-3
37 Teoh, S.S.Y., Wang, Y., Li, Y., Leemaqz, S.Y.L., Dekker, G.A., Roberts, C.T. et al. (2019) Low serum levels of HtrA3 at 15 weeks of gestation are associated with late-onset preeclampsia development and small for gestational age birth. *Fetal Diagn. Ther.* **46**, 392–401 https://doi.org/10.1159/000497144
38 Bowden, M.A., Di Nezza-Cossens, L.A., Jobling, T., Salamonsen, L.A. and Nie, G. (2006) Serine proteases HTRA1 and HTRA3 are down-regulated with increasing grades of human endometrial cancer. *Gynecol. Oncol.* **103**, 253–260 https://doi.org/10.1016/j.ygyno.2006.03.006
39 Narkiewicz, J., Klasa-Mazurkiewicz, D., Zurawa-Janicka, D., Skorko-Glonek, J., Emerich, J. and Lipinska, B. (2008) Changes in mRNA and protein levels of human HtrA1, HtrA2 and HtrA3 in ovarian cancer. *Clin. Biochem.* **41**, 561–569 https://doi.org/10.1016/j.clinbiochem.2008.01.004
40 Ongenaert, M., Wisman, G.B.A., Volders, H.H., Koning, A.J., Zee, A.G., van Criekinge, W. et al. (2008) Discovery of DNA methylation markers in cervical cancer using relaxation ranking. *BMC Med. Genom.* **1**, 57 https://doi.org/10.1186/1755-8794-1-57
41 Beleford, D., Rattan, R., Chien, J. and Shridhar, V. (2010) High temperature requirement A3 (HtrA3) promotes etoposide- and cisplatin-induced cytotoxicity in lung cancer cell lines. *J. Biol. Chem.* **285**, 12011–12027 https://doi.org/10.1074/jbc.M109.097790
42 Jacobson, M.P., Pincus, D.L., Rapp, C.S., Day, T.J.F., Honig, B., Shaw, D.E. et al. (2004) A hierarchical approach to all-atom protein loop prediction. *Proteins* **55**, 351–367 https://doi.org/10.1002/prot.10613
43 Jacobson, M.P., Friesner, R.A., Xiang, Z. and Honig, B. (2002) On the role of the crystal environment in determining protein side-chain conformations. *J. Mol. Biol.* **320**, 597–608 https://doi.org/10.1016/S0022-2836(02)00470-9
44 Li, W., Srinivasula, S.M., Chai, J., Li, P., Wu, J.-W., Zhang, Z. et al. (2002) Structural insights into the pro-apoptotic function of mitochondrial serine protease HtrA2/Omi. *Nat. Struct. Biol.* **9**, 436–441 https://doi.org/10.1038/nsb795
45 Abraham, M.J., Murtola, T., Schulz, R., Páll, S., Smith, J.C., Hess, B. et al. (2015) GROMACS: high performance molecular simulations through multi-level parallelism from laptops to supercomputers. *SoftwareX.* **1–2**, 19–25 https://doi.org/10.1016/j.softx.2015.06.001
46 Aliev, A.E., Kulke, M., Khaneja, H.S., Chudasama, V., Sheppard, T.D. and Lanigan, R.M. (2014) Motional timescale predictions by molecular dynamics simulations: case study using proline and hydroxyproline sidechain dynamics. *Proteins* **82**, 195–215 https://doi.org/10.1002/prot.24350
47 Mark, P. and Nilsson, L. (2001) Structure and dynamics of the TIP3P, SPC, and SPC/E water models at 298K. *J. Phys. Chem. A* **105**, 9954–9960 https://doi.org/10.1021/jp003020w
48 Wardi, Y. (1988) A stochastic steepest-descent algorithm. *J. Optim. Theory Appl.* **59**, 307–323 https://doi.org/10.1007/BF00938315
49 Kawata, M. and Nagashima, U. (2001) Particle mesh Ewald method for three-dimensional systems with two-dimensional periodicity. *Chem. Phys. Lett.* **340**, 165–172 https://doi.org/10.1016/S0009-2614(01)00393-1
50 Hünenberger, P.H. (2005) Thermostat algorithms for molecular dynamics simulations. *Adv. Comput. Simul.* **173**, 105–149 https://doi.org/10.1007/b99427
51 Meinhold, L., Smith, J.C., Kitao, A. and Zewail, A.H. (2007) Picosecond fluctuating protein energy landscape mapped by pressure temperature molecular dynamics simulation. *Proc. Natl Acad. Sci. U.S.A.* **104**, 17261–5 https://doi.org/10.1073/pnas.0708199104
52 McDonald, I.R. (1972) NpT-ensemble Monte Carlo calculations for binary liquid mixtures. *Mol. Phys.* **23**, 41–58 https://doi.org/10.1080/00268977200100031
53 Hess, B., Bekker, H., Berendsen, H.J.C. and Fraaije, J.G.E.M. (1997) LINCS: a linear constraint solver for molecular simulations. *J. Comput. Chem.* **18**, 1463–1472 https://doi.org/10.1002/(SICI)1096-987X(199709)18:12<1463::AID-JCC4>3.0.CO;2-H
54 Maisuradze, G.G., Liwo, A. and Scheraga, H.A. (2010) Relation between free energy landscapes of proteins and dynamics. *J. Chem. Theory Comput.* **6**, 583–595 https://doi.org/10.1021/ct9005745
55 Kim, S., Grant, R.A. and Sauer, R.T. (2011) Covalent linkage of distinct substrate degrons controls assembly and disassembly of DegP proteolytic cages. *Cell* **145**, 67–78 https://doi.org/10.1016/j.cell.2011.02.024
56 Runyon, S.T., Zhang, Y., Appleton, B.A., Sazinsky, S.L., Wu, P., Pan, B. et al. (2007) Structural and functional analysis of the PDZ domains of human HtrA1 and HtrA3. *Protein Sci.* **16**, 2454–2471 https://doi.org/10.1110/ps.073049407
57 Bahar, I., Atilgan, A.R., Demirel, M.C. and Erman, B. (1998) Vibrational dynamics of folded proteins: significance of slow and fast motions in relation to function and stability. *Phys. Rev. Lett.* **80**, 2733–2736 https://doi.org/10.1103/PhysRevLett.80.2733
58 Babu M, M., Singh S, K. and Balaram, P. (2002) A C–H···O hydrogen bond stabilized polypeptide chain reversal motif at the C terminus of helices in proteins. *J. Mol. Biol.* **322**, 871–880 https://doi.org/10.1016/S0022-2836(02)00715-5
59 Sohn, J., Grant, R.A. and Sauer, R.T. (2010) Allostery is an intrinsic property of the protease domain of DegS: implications for enzyme function and evolution. *J. Biol. Chem.* **285**, 34039–34047 https://doi.org/10.1074/jbc.M110.135541
60 Srinivasula, S.M., Gupta, S., Datta, P., Zhang, Z., Hegde, R., Cheong, N. et al. (2003) Inhibitor of apoptosis proteins are substrates for the mitochondrial serine protease Omi/HtrA2. *J. Biol. Chem.* **278**, 31469–31472 https://doi.org/10.1074/jbc.C300240200
61 Wenta, T., Rychlowski, M., Jurewicz, E., Jarzab, M., Zurawa-Janicka, D., Filipek, A. et al. (2019) The HtrA3 protease promotes drug-induced death of lung cancer cells by cleavage of the X-linked inhibitor of apoptosis protein (XIAP). *FEBS J.* **286**, 4579–4596 https://doi.org/10.1111/febs.14977

62 Wenta, T., Zurawa-Janicka, D., Rychlowski, M., Jarzab, M., Glaza, P., Lipinska, A. et al. (2018) Htra3 is a cellular partner of cytoskeleton proteins and TCP1α chaperonin. *J. Proteom.* **177**, 88–111 https://doi.org/10.1016/j.jprot.2018.02.022
63 Truebestein, L., Tennstaedt, A., Mönig, T., Krojer, T., Canellas, F., Kaiser, M. et al. (2011) Substrate-induced remodeling of the active site regulates human HTRA1 activity. *Nat. Struct. Mol. Biol.* **18**, 386–388 https://doi.org/10.1038/nsmb.2013
64 Walle L, V., Van Damme, P., Lamkanfi, M., Saelens, X., Vandekerckhove, J., Gevaert, K. et al. (2007) Proteome-wide identification of HtrA2/Omi substrates. *J. Proteome Res.* **6**, 1006–1015 https://doi.org/10.1021/pr060510d
65 Martins, L.M., Turk, B.E., Cowling, V., Borg, A., Jarrell, E.T., Cantley, L.C. et al. (2003) Binding specificity and regulation of the serine protease and PDZ domains of HtrA2/Omi. *J. Biol. Chem.* **278**, 49417–49427 https://doi.org/10.1074/jbc.M308659200
66 Zhang, X. and Chang, Z. (2004) Temperature dependent protease activity and structural properties of human HtrA2 protease. *Biochemistry (Moscow)* **69**, 687–692 https://doi.org/10.1023/B:BIRY.0000033743.09806.1a
67 Li, Y., Puryer, M., Lin, E., Hale, K., Salamonsen, L.A., Manuelpillai, U. et al. (2011) Placental HtrA3 is regulated by oxygen tension and serum levels are altered during early pregnancy in women destined to develop preeclampsia. *J. Clin. Endocrinol. Metab.* **96**, 403–411 https://doi.org/10.1210/jc.2010-1405
68 Singh, H., Si, M., Endo, Y. and Nie, G. (2010) Inhibition of HTRA3 stimulates trophoblast invasion during human placental development. *Placenta* **31**, 1085–1092 https://doi.org/10.1016/j.placenta.2010.10.003